



DTIC
ELECTE
JAN 05 1995
S G D

VISCOPLASTIC CHARACTERIZATION AND
FATIGUE MODELING OF TITANIUM BASED
METAL MATRIX COMPOSITES

THESIS

Mark A. Foringer, Capt, USAF

AFIT/GAE/ENY/94D-5

19950103 077

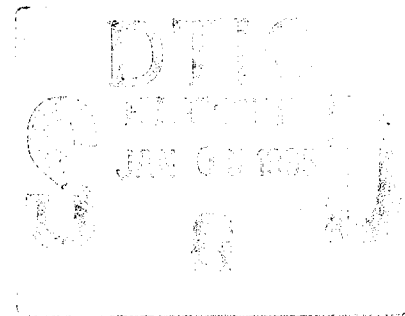
DEPARTMENT OF THE AIR FORCE
AIR UNIVERSITY
AIR FORCE INSTITUTE OF TECHNOLOGY

Wright-Patterson Air Force Base, Ohio

DISTRIBUTION STATEMENT A

Approved for public release;

Accession For	
NTIS CRA&I	<input checked="" type="checkbox"/>
DTIC TAB	<input type="checkbox"/>
Unannounced	<input type="checkbox"/>
Justification	
By	
Distribution /	
Availability Codes	
Dist	Avail and/or Special
A-1	



VISCOPLASTIC CHARACTERIZATION AND
FATIGUE MODELING OF TITANIUM BASED
METAL MATRIX COMPOSITES

THESIS

Mark A. Foringer, Capt, USAF

AFIT/GAE/ENY/94D-5

DTIC QUALITY INSPECTED 2

Approved for public release; distribution unlimited

The views expressed in this thesis are those of the author and do not reflect the official policy or position of the Department of Defense or the U. S. Government.

VISCOPLASTIC CHARACTERIZATION AND FATIGUE MODELING OF
TITANIUM BASED METAL MATRIX COMPOSITES

THESIS

Presented to the Faculty of the School of Engineering

Air Force Institute of Technology

Air Education and Training Command

In Partial Fulfillment of the

Requirements for the Degree of

Master of Science in Aeronautical Engineering

Mark A. Foringer, B.S., MBA

Captain, USAF

December 1994

Approved for public release; distribution unlimited

Acknowledgments

I am indebted to several people for the completion of this effort. Mark Derisso was invaluable in guiding me through the operations of the tensile testing equipment. Capt Craig Steiner and Lt Darren Kraabel were also very helpful in discussing ideas about both fatigue modeling and computer operations. Their advice definitely contributed to the overall success this study. Thanks also go to Lt Col John Rogacki for providing the raw data for titanium 15-3 at elevated temperatures. I'd also like to thank Dr. Jones of AFOSR for providing the necessary material to accomplish the experimental work.

Most of all, I am indebted to my advisor, Capt David Robertson. He provided insight and guidance throughout the course of my thesis. He allowed me to develop the fatigue theories using my own ideas with only minor course corrections. This level of oversight let me develop ideas desired by the Aeronautical Engineering Department as well as letting me go my own way.

Mark A. Foringer

Table of Contents

	Page
Preface.....	ii
List of Figures.....	v
List of Tables.....	viii
List of Symbols.....	ix
Abstract.....	xi
I. Introduction.....	1
II. Background.....	5
2.1 Viscoplasticity.....	5
2.1.1 Internal State Variables.....	7
2.1.2 The Miller Model.....	7
2.1.3 The Walker Model.....	8
2.1.4 The Bodner-Partom Model.....	8
2.2 Micromechanics.....	11
2.3 Fatigue Life Models.....	13
2.4 Experimental Work.....	17
III. Methodology.....	20
3.1 Viscoplastic Characterization of Ti-15-3.....	20
3.1.1 Experimental Procedure.....	21
3.1.2 Constant Determination.....	22
3.2 Embedding Micromechanics into Existing Model.....	25
3.3 Constituent Behavior Based Model.....	26
IV. Results and Discussion.....	28
4.1 Characterization of Titanium 15-3.....	29
4.1.1 Experimental Results.....	29
4.1.2 Viscoplastic Characterization.....	32
4.1.3 Micromechanics Application.....	40
4.1.4 Viscoplastic Discussion.....	42

4.2 Linear Damage Accumulation Model.....	45
4.2.1 SCS-6/Ti- β 21s Cross Ply Isothermal Microstresses.....	46
4.2.2 SCS-6/Ti- β 21s Cross Ply Isothermal Fatigue.....	49
4.2.3 SCS-6/Ti- β 21s Cross Ply Thermomechanical Fatigue.....	50
4.2.4 TMF Modeling of Other SCS-6/Ti- β 21s Lay-ups.....	51
4.2.5 SCS-6/Ti-15-3 Cross Ply Isothermal Fatigue.....	54
4.2.6 SCS-6/Ti-15-3 Laminate Thermomechanical Fatigue.....	55
4.2.7 Linear Damage Accumulation Model Discussion.....	57
4.3 Constituent Based Model.....	65
4.3.1 Matrix Fatigue Behavior.....	66
4.3.2 Fiber and 0° Ply Fatigue Behavior.....	67
4.3.3 Interface and 90° Fatigue Behavior.....	69
4.3.4 Cross Ply Fatigue Behavior.....	71
4.3.5 Constituent Fatigue Model Discussion.....	72
4.4 Consolidated Constants Tables.....	74
4.4.1 Bodner-Partom Viscoplastic Constants (Ti-15-3).....	74
4.4.2 Linear Damage Accumulation Model Constants.....	75
4.4.3 Constituent Based Model Constants.....	75
V. Conclusions and Recommendations.....	76
5.1 Conclusions.....	76
5.2 Recommendations for Future Research.....	78
VI. References.....	80
Appendix A.....	84
Vita.....	90

List of Figures

Figure	Page
1. Representative Volume Element and Analysis Cell.....	12
2. Ti-15-3, Room Temperature.....	29
3. Ti-15-3, 315°C.....	30
4. Ti-15-3, 427°C.....	30
5. Poisson's Ratio for Ti-15-3.....	31
6. Ti-15-3, Room Temp, .001/s.....	33
7. Ti-15-3, 315°C, .01/s.....	34
8. Ti-15-3, 315°C, .0001/s.....	34
9. Ti-15-3, 427°C, .01/s.....	35
10. Ti-15-3, 427°C, .0001/s.....	35
11. Ti-15-3, 482°C, .01/s.....	36
12. Ti-15-3, 482°C, .0001/s.....	37
13. Ti-15-3, 566°C, .01/s.....	37
14. Ti-15-3, 566°C, .0001/s.....	38
15. Ti-15-3, 649°C, .01/s.....	38
16. Ti-15-3, 649°C, .0001/s.....	39
17. Angle Ply, Stress-Strain, 427°C.....	40
18. Angle Ply, Max-Min Strain History Under Isothermal Fatigue (Max Stress = 300 MPa), 427°C.....	41
19. Ti-15-3, Z_2 & Z_3 vs Temperature.....	44
20. SCS-6/Ti- β 21s Cross Ply Fiber Microstress vs Cycle, 650°C Isothermal.....	47

Figure	Page
21. SCS-6/Ti- β 21s Cross Ply Matrix Microstress vs Applied Stress, 650°C Isothermal.....	48
22. SCS-6/Ti- β 21s Cross Ply, 650°C Isothermal.....	49
23. SCS-6/Ti- β 21s Cross Ply Fiber Stresses, In-Phase & Out-of-Phase TMF, 3 Min 150°C/650°C Cycles.....	50
24. SCS-6/Ti- β 21s Cross Ply, 150°C/650°C TMF.....	51
25. SCS-6/Ti- β 21s Quasi-Isotropic, 150°C/650°C TMF.....	52
26. SCS-6/Ti- β 21s Unidirectional, 150°C/650°C TMF.....	52
27. SCS-6/Ti- β 21s Unidirectional, TMF, Revised n_m	53
28. SCS-6/Ti-15-3 Cross Ply, 427°C Isothermal.....	54
29. SCS-6/Ti-15-3 Cross Ply Fiber Stresses, 149°C/427°C TMF.....	55
30. SCS-6/Ti-15-3 Cross Ply, 149°C/427°C TMF.....	56
31. SCS-6/Ti-15-3 Quasi-Isotropic, 149°C/427°C TMF.....	57
32. SCS-6/Ti- β 21s Cross Ply, 650°C Isothermal, N_{pred} vs N_{exp}	58
33. SCS-6/Ti-15-3 Cross Ply, Isothermal N_{pred} vs N_{exp}	59
34. SCS-6/Ti- β 21s Cross Ply, TMF N_{pred} vs N_{exp}	60
35. SCS-6/Ti-15-3 Cross Ply, TMF N_{pred} vs N_{exp}	61
36. SCS-6/Ti- β 21s Quasi-Isotropic, TMF N_{pred} vs N_{exp}	62
37. SCS-6/Ti-15-3 Quasi-Isotropic, TMF N_{pred} vs N_{exp}	62
38. SCS-6/Ti- β 21s Unidirectional, TMF N_{pred} vs N_{exp}	64
39. Ti-15-3, Isothermal Fatigue S-N, 25°C.....	66
40. SCS-6, Isothermal Fatigue Model, 25°C.....	68
41. SCS-6/Ti-15-3 0° Ply, Isothermal Fatigue, 25°C.....	68
42. SCS-6/Ti-15-3 90° Ply, Interface Damage, Iso. Fatigue, 25°C.....	70

Figure	Page
43. SCS-6/Ti-15-3 90° Ply, Isothermal Fatigue, 25°C.....	70
44. SCS-6/Ti-15-3 Cross Ply Lamina Stresses.....	71
45. SCS-6/Ti-15-3 Cross Ply, Isothermal Fatigue, 25°C, Individual Lamina Predictions.....	73

List of Tables

Table	Page
1. SCS-6/Ti- β 21s Fatigue Data.....	19
2. SCS-6/Ti-15-3 Fatigue Data.....	19
3. Temp. Dependent Bodner-Partom Constants.....	32
4. Temp. Dependent Bodner-Partom Constants.....	74
5. Linear Damage Accumulation Model Constants.....	75
6. Constituent Based Model Constants.....	75

List of Symbols

Symbol	Description
A.....	Empirical Constant in Cyclic Damage Term
α	Thermal Expansion Coefficient
a_1	Bodner-Partom Constant
a_2	Bodner-Partom Constant
a_n	General Viscoelastic Constant
B.....	Empirical Constant in Time to Failure Term
β	Directional Hardening Factor
b_m	General Viscoelastic Constant
B_m, B	Empirical Constant in Matrix Damage Term
C.....	Empirical Constant in Cycle-Term Interaction Term
C_u	Interfacial Damage Material Constant
D_0	Bodner-Partom Constant
δ_I	Interface Damage Factor
E.....	Elastic Modulus
ϵ	Strain
ϵ^E	Elastic Strain
ϵ^{TH}	Thermal Strain
ϵ^P	Plastic Strain
ϵ^{CR}	Strain Due to Creep
ϵ^I	Inelastic Strain
f.....	Frequency
F.....	Fatigue Model Scale Factor
J_2	2nd Invariant of Deviatoric Stress
k.....	Viscoplastic Algorithm Convergence Term
m_1	Bodner-Partom Constant
m_2	Bodner-Partom Constant
n.....	Bodner-Partom Constant
n_m, n	Empirical Constant in Matrix Damage Term
n	Empirical Constant for Time to Failure Term
N.....	Fatigue Life in Cycles until Failure
ν	Poisson's Ratio
N_c	Cyclic Damage Term
N_t	Time Dependent Damage Term
N_i	Cycle/Time Interaction Term
N_m	Matrix Damage Term
N_f	Fiber Damage Term
N_i	Interface Degradation Term
N_0	Empirical Constant in Fiber Damage Term
p.....	Empirical Constant in Fiber Damage Term
R.....	Load Ratio
r_1	Bodner-Partom Constant

Symbol	Description
r_2	Bodner-Partom Constant
σ	Stress
S	Standard Deviation of Interfacial Stress Distribution
σ_m	Mean Interfacial Stress
σ_f	Fiber Stress
σ_I	Interfacial Stress
σ_m	Matrix Stress
S_{ij}	Deviatoric Stress
σ_0	Empirical Constant in Fiber Damage Term
t	Time
T	Temperature
t_c	Time to Failure Under Constant Stress
W_p	Plastic Work
y	Geometric Averaging Weight Factor
z	Geometric Averaging Weight Factor
Z	Drag Stress
Z^D	Directional Hardening Term
Z^I	Isotropic Hardening Term
Z_0	Bodner-Partom Constant
Z_1	Bodner-Partom Constant
Z_2	Bodner-Partom Constant
Z_3	Bodner-Partom Constant

Abstract

Viscoplastic characterization and fatigue modeling of titanium-based metal matrix composites (MMCs) was accomplished by combining a unified viscoplastic theory, a nonlinear micromechanics model, and a linear damage accumulation model. For the viscoplastic characterization, constant strain rate tension tests were performed on the titanium 15-3 matrix. Ti-15-3 was then successfully characterized using the Bodner-Partom viscoplastic theory with directional hardening. Subsequently, the new parameters required for this theory for Ti-15-3 as well as previously determined parameters for titanium β 21s were incorporated into the micromechanics model, and results from this model demonstrated excellent correlation with the known material response of the MMC. Microstress information extracted from the micromechanics was then employed in a linear damage accumulation fatigue model. This successfully accounted for the time-dependent fatigue behavior of silicon carbide fiber and titanium β 21s composites for isothermal fatigue at 650°C, in phase thermomechanical fatigue (150°C-650°C), and out of phase thermomechanical fatigue (150°C-650°C). The laminates modeled were $[0]_4$, $[0/90]_s$, and $[0/\pm 45/90]_s$. A new linear damage accumulation model was developed based on the fatigue behavior of the constituents of the composite. This model was applied to unidirectional and cross-ply SCS-6/Ti-15-3 laminates at room temperature and 427°C. Both models can be used to produce at least an estimate of the fatigue behavior of titanium matrix composites.

VISCOPLASTIC CHARACTERIZATION AND FATIGUE MODELING OF TITANIUM BASED METAL MATRIX COMPOSITES

I. Introduction

In recent years, composites have received a lot of attention in a wide variety of uses. Continuous fiber reinforced composites have been extensively examined since they are generally very strong in the fiber direction. Historically, polymeric composites have dominated this field. In such composites, the fibers carried the vast majority of the load, and the matrix was present just to hold the fibers in place. This yielded a lamina that was very strong in uniaxial tension along the fiber axis, but very weak in transverse tension or shear. Another disadvantage is that the matrix material (usually an epoxy compound) had a low melting temperature. Thus, these composites were poorly suited to high temperature applications. Since there are many aerospace requirements for performance at elevated temperatures, epoxy composites have limited use in the aerospace field. As a result, more robust composite matrix materials such as ceramics and metals were required.

Titanium based metal matrix composites have been the focus of study in recent years and show good promise in high temperature composite uses. Two such systems have been tested significantly in the last few years. The first is TIMETAL®21S, also known as titanium β 21s (Ti-15Mo-3Nb-3Al-0.2Si wt-%). The second is titanium 15-3 (Ti-15V-3Cr-3Al-3Sn). Both of these alloys maintain workable mechanical properties up to about 800°C and have been successfully combined with silicon carbide fibers (SCS-6) to form viable metal matrix composites.

Although metal matrix composites (MMCs) solve the problem of operating at elevated temperatures, they introduce many other factors which must be resolved before being put into use. One of these characteristics is the fact that the matrix material in an MMC has comparable strength to that of the fiber material. This is contradictory to the behavior of epoxy matrix composites used in the past. In an epoxy matrix composite, failure of the composite is based almost entirely on the failure of the fibers. Since the matrix material can hold a more equal percentage of the load in an MMC, composite failure is more complex. This even load distribution results in a greater importance of the micromechanical interaction between the fibers and the matrix.

Another trait of MMCs which must be understood is the nature of the matrix material itself. Since the matrix material is metallic, it usually exhibits some degree of inelastic behavior, making analysis substantially more difficult. Many of the metals being examined as matrix materials are relatively new alloys and viscoplastic characterization is incomplete. To accurately predict the fatigue behavior of MMCs, it is necessary to model the micromechanical behavior of the composite as well as the viscoplastic behavior of the matrix material.

The present study has 3 distinct phases. The objective of the first phase is to determine the viscoplastic material constants for Titanium 15-3 at temperatures ranging from 25°C to 700°C using the Bodner Partom theory with directional hardening [1, 2] based on experimental constant strain rate data. In order to span the entire temperature range, experimental data from a previous study [3] are combined with the data obtained under the present effort. These parameters will then be integrated into a micromechanics

model [4] to accurately predict behavior of a titanium matrix composite under a variety of mechanical and thermal loading cycles.

The second phase of the present study will attempt to modify an existing fatigue behavior model [5-8] by removing the time dependent damage terms. The information in these terms will be replaced by information from the micromechanics model which accounts for the time dependent viscoplastic behavior of the matrix material. Results from the model are compared to data for titanium β 21s matrix composite fatigue data for different frequencies in both isothermal and thermomechanical fatigue. Since the model to be modified is purely empirical, removing the time dependent terms will reduce the number of parameters required to predict the composite's behavior. Additionally, allowing the micromechanics model to address the time dependency through viscoplastic behavior theory results in a more physically based model.

Most fatigue prediction models (including the model used in phase II of this study) rely on empirical curve fitting to experimental data. The constants involved have little relation to the physical properties of the constituents. The goal of the third phase is, therefore, to develop a new model based on the physical constituent properties of a titanium 15-3 matrix composite. This model would predict composite fatigue behavior of a lamina based on the behavior of the matrix material, the fibers, and the interface region. It would then predict behavior of a laminate by that of each of the layers. Results from the model are compared with isothermal fatigue data for titanium 15-3 matrix composites.

A model based on the physical properties of a composite's individual components has many advantages. It is easier and more intuitive to determine the properties of each

individual component, and then combine these in a relatively straight forward manner than empirically establishing a set of different constants which might change for each new loading combination. Additionally, a model based on the behavior of the constituents will be more apt to work for a variety of materials with little alteration.

In the present study, the two models discussed in phases II and III are presented as simple approaches for predicting the fatigue life of metal matrix composites. The more complicated attributes of viscoplasticity and time dependency are handled by the micromechanics model. Both fatigue prediction models prove to work fairly well at modeling the existing experimental data.

II. Background

Titanium matrix composites have recently received significant attention for use in high temperature aerospace applications because of high stiffness and strength characteristics at elevated temperatures. The use of metal as a matrix, however, introduces several new difficulties when attempting to predict the composite's behavior under either static or cyclic load. Since the properties of the metal matrix are comparable to the properties of the silicon carbide fibers, the behavior of the matrix material can no longer be neglected as in classical composite behavior theory. Thus, it is necessary to be able to predict the behavior of the constituents at the micromechanical level to successfully predict the behavior of the composite. This requires knowledge of how the fiber material and the matrix material behave under load.

Although the fiber material can be modeled as a linear elastic material due to its brittleness, this is not true for the metal matrix material. Like most metals, titanium exhibits linear elastic behavior at stresses below its yield point, but demonstrates plastic behavior above yield. Therefore, a more complicated micromechanical model with the capability to handle viscoplastic effects is required to predict the material's behavior.

2.1 Viscoplasticity

Time-dependent material behavior is generally accounted for by assuming the material represents either viscoelastic or viscoplastic response. These two theories model unique material responses. Viscoelastic theories improve on linear elastic theories by taking into account the effects of strain rates in the form of creep and stress relaxation.

Viscoelasticity is discussed in texts at the graduate level [9]. Generally, viscoelastic behavior can be expressed as in Equation (1) [10]:

$$\sum_{m=0}^M b_m \frac{d^m}{dt^m} \sigma(t) = \sum_{n=0}^N a_n \frac{d^n}{dt^n} \epsilon(t) \quad (1)$$

where σ is stress, ϵ is strain, and the a 's and b 's are material constants. Several researchers have proposed a more advanced variation of this theory with the integer derivative being replaced by one of fractional order [10, 11]. Since viscoelasticity theory accounts for time dependent behavior, it will generally be more accurate than linear elastic theory. However, it requires the solution of potentially complicated differential equations and still does not address inelastic behavior.

Viscoplastic theories seek to model the time-dependent material behavior in the plastic realm. As a result, they can be very complicated and often do not yield a closed form solution. Viscoplastic theories can be generally divided into two subsets: classical and unified. Classical viscoplastic theories generally separate the total strain rate into four terms as follows:

$$\dot{\epsilon}_{ij}^{TOT} = \dot{\epsilon}_{ij}^E + \dot{\epsilon}_{ij}^{TH} + \dot{\epsilon}_{ij}^P + \dot{\epsilon}_{ij}^{CR} \quad (2)$$

where ϵ^E is elastic strain, ϵ^{TH} is thermal strain, ϵ^P is plastic strain, and ϵ^{CR} is strain due to creep. In contrast, unified viscoplastic theories combine the creep and plastic strain terms into a single inelastic strain term:

$$\dot{\epsilon}_{ij}^{TOT} = \dot{\epsilon}_{ij}^E + \dot{\epsilon}_{ij}^{TH} + \dot{\epsilon}_{ij}^I \quad (3)$$

where ϵ^I is inelastic strain. There are many viscoplastic theories of material behavior in literature, but only three unified models will be discussed in the present document: the

Miller, Walker, and Bodner-Partom theories [3, 12-17].

2.1.1 Internal State Variables [3]

Each of the three unified viscoplastic theories discussed in the present effort have a number of state variables such as applied stress, elastic modulus, etc. In addition, the models also have at least two internal state variables. For the three theories discussed here, the internal state variables are inelastic strain, back stress, and drag stress. Inelastic strain is defined as the total strain minus the elastic and thermal strains. Back stress is used to account for kinematic hardening. During inelastic deformation, dislocations accumulate on the slip planes in the material resisting the applied stress. When the loading is reversed, the amassed dislocations aid in movement. Drag stress corresponds to the average dislocation density, which leads to isotropic hardening. Drag stress also accounts for cyclic hardening or softening of the material.

2.1.2 The Miller Model [12]

The Miller model of viscoplasticity is strongly related to underlying microscopic physical mechanisms. It is based on a single hyperbolic sine strain rate function and two equations to account for work-hardening and recovery. The three independent state variables (ISVs) in the Miller model are inelastic strain, rest (or back) stress, and drag stress. Since a single strain rate equation generates all of the inelastic strain, the model is unified. The Miller model requires the determination of ten constants to model viscoplastic behavior of a material, not including the elastic modulus, E . It is difficult to characterize a material using this model because it requires cyclic constant strain rate tests

which are difficult to perform [3].

2.1.3 The Walker Model [13, 3]

The Walker model is based on a nonlinear modification to a three-parameter solid comprised of a spring and Voigt element in series. Like the Miller model, it is a unified theory with three ISVs: back stress, drag stress, and inelastic strain. The Walker theory requires 16 material parameters to model viscoplastic behavior. With several assumptions, the number of constants required to characterize a material using this model can be reduced to 9. However, like the Miller model, the Walker model requires the use of cyclic constant strain rate tests to provide the experimental basis [3].

2.1.4 The Bodner-Partom Model

The Bodner-Partom theory was originally proposed as a unified viscoplastic theory with inelastic strain and drag stress as the only two ISVs [1]. It assumes isotropic behavior and isothermal loading. Later efforts modify the original Bodner-Partom theory to include kinematic hardening, back stress, and nonisothermal effects [2, 14-17]. The basic Bodner-Partom theory can be represented in three dimensions by these equations:

$$\dot{\epsilon}_{ij}^I = D_0 \frac{S_{ij}}{\sqrt{J_2}} \exp \left[-\frac{(n+1)}{2n} \left(\frac{Z^2}{3J_2} \right)^n \right] \quad (4)$$

$$\dot{Z} = m \dot{W}_p \frac{(Z_1 - Z)}{Z_0} \quad (5)$$

$$\dot{W}_p = \sigma_{ij} \dot{\epsilon}_{ij}^I \quad (6)$$

where S_{ij} is deviatoric stress, J_2 is the second invariant of deviatoric stress, Z is the state

variable drag stress, W_p is plastic work, and the remaining undefined terms are material constants.

When the basic theory is modified to include directional hardening and nonisothermal effects, the equations are changed to the following:

$$\dot{\epsilon}_{ij}^I = D_0 \frac{S_{ij}}{\sqrt{J_2}} \exp \left[-\frac{1}{2} \left(\frac{(Z^I + Z^D)^2}{3J_2} \right)^n \right] \quad (7)$$

where the major alteration is the separation of the drag stress, Z , into two terms, Z^I and Z^D . Z^I represents the isotropic hardening effects, and Z^D represents the directional hardening effects. Z^I and Z^D are given by:

$$\begin{aligned} \dot{Z}^I = & m_1 \dot{W}_p (Z_1 - Z^I) - A_1 Z_1 \left(\frac{Z^I - Z_2}{Z_1} \right)^{r_1} \\ & + \dot{T} \left[\left(\frac{Z^I - Z_2}{Z_1 - Z_2} \right) \frac{\partial Z_1}{\partial T} + \left(\frac{Z_1 - Z^I}{Z_1 - Z_2} \right) \frac{\partial Z_2}{\partial T} \right] \end{aligned} \quad (8)$$

$$Z^D = \beta_{ij} u_{ij} \quad (9)$$

$$\begin{aligned} \dot{\beta}_{ij} = & m_2 \dot{W}_p (Z_3 u_{ij} - \beta_{ij}) \\ & - A_2 Z_1 \frac{\beta_{ij}}{\sqrt{\beta_{kl} \beta_{kl}}} \left(\frac{\sqrt{\beta_{kl} \beta_{kl}}}{Z_1} \right)^{r_2} + \dot{T} \frac{\beta_{ij}}{Z_3} \frac{\partial Z_3}{\partial T} \end{aligned} \quad (10)$$

$$u_{ij} = \frac{\sigma_{ij}}{\sqrt{\sigma_{kl} \sigma_{kl}}} \quad (11)$$

where all terms defined earlier keep those definitions, and the new terms are additional material constants.

For unidirectional loading, the Bodner-Partom theory with directional hardening simplifies to the following equations:

$$\sigma = E(\epsilon - \epsilon_I - \epsilon_T) \quad (12)$$

$$\dot{\epsilon}_I = \frac{2D_0}{\sqrt{3}} \exp \left[-\frac{1}{2} \left(\frac{Z^I + Z^D}{\sigma} \right)^{2n} \right] \quad (13)$$

$$\begin{aligned} \dot{Z}^I = m_1 \dot{W}_p - A_1 Z_1 \left(\frac{Z^I - Z_2}{Z_1} \right)^{r_1} \\ + \dot{T} \left[\left(\frac{Z^I - Z_2}{Z_1 - Z_2} \right) \frac{\partial Z_1}{\partial T} + \left(\frac{Z_1 - Z^I}{Z_1 - Z_2} \right) \frac{\partial Z_2}{\partial T} \right] \end{aligned} \quad (14)$$

$$\dot{Z}^D = m_2 \dot{W}_p (Z_3 - Z^D) - A_2 Z_1 \left(\frac{Z^D}{Z_1} \right)^{r_2} + \dot{T} \frac{Z^D}{Z_3} \frac{\partial Z_3}{\partial T} \quad (15)$$

$$\dot{W}_p = \sigma \dot{\epsilon}_I \quad (16)$$

where all terms are as defined previously. All the material properties, except for D_0 , but including E , are dependent upon temperature. It is this form of the Bodner-Partom theory which is used in the present effort.

Researchers have found that the Bodner-Partom model is the easiest to use to characterize the viscoplastic behavior of titanium alloys for two reasons: there is a procedure available to find the constants [18], and the experiments required (constant strain rate tests) are relatively easy to perform [3]. The modified Bodner-Partom theory is used in the present study both directly in the determination of constants to characterize titanium 15-3 and indirectly through the use of the micromechanics model.

2.2 Micromechanics

To predict the behavior of a composite, it is necessary to understand how the constituents of the composite behave micromechanically. This is especially true for metal matrix composites. There have been several micromechanical models developed in recent years to predict the behavior of metal matrix composites. One approach is to model the composite as a finite element mesh with the elements having the properties of the fiber or the matrix as appropriate [19]. Other models use some elements of the mesh to model the interface between the fiber and matrix, but use matrix properties to characterize the interface [20]. Still others attempt to model the interface as a distinct entity which has unique properties which model the debonding or slippage that occurs during composite loading [4, 21-23].

The present study uses one of these latter types of models to provide the micromechanical predictions of titanium matrix composites. The model was developed at the Air Force Institute of Technology by Robertson and Mall [4, 23]. It is based on an Aboudi unit cell [24] as shown in Figure 1. The stresses in each of the four regions is assumed to be constant. The model uses the Bodner-Partom theory of viscoplasticity to characterize the matrix material. It treats the fiber material as linear elastic and allows for damage in the interface between the fiber and matrix.

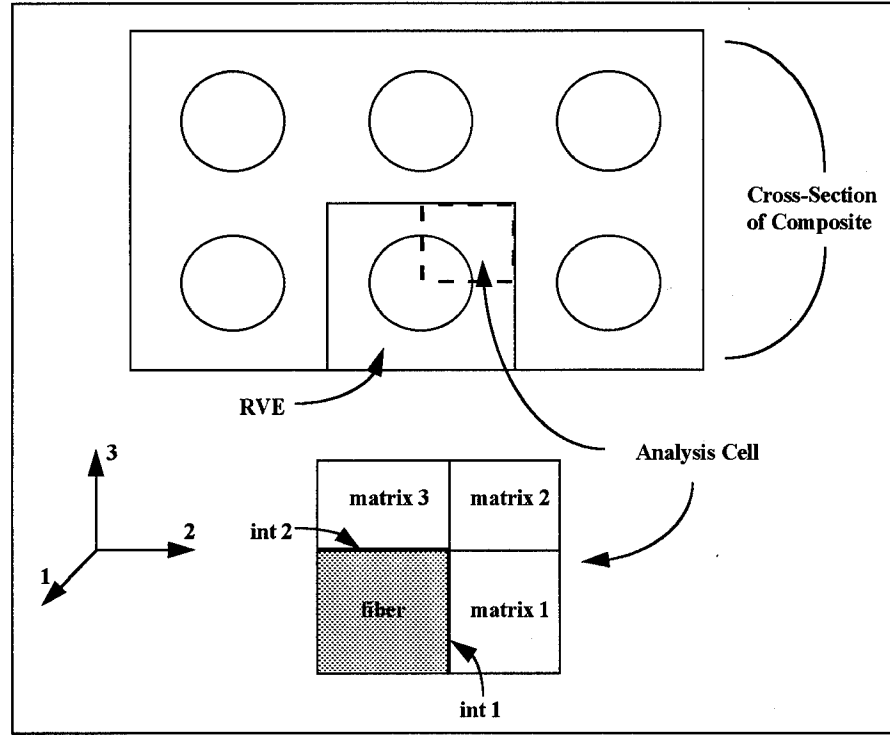


Figure 1. Representative Volume Element and Analysis Cell

The laminate analysis is achieved by employing the classical laminated plate and assembling the nonlinear constitutive relations from each ply into a global laminate nonlinear equation. The general form of the assembled equation is:

$$\begin{bmatrix} \mathbf{P} \end{bmatrix} \begin{Bmatrix} {}_0\boldsymbol{\varepsilon} \\ \boldsymbol{\kappa} \\ \boldsymbol{\sigma}_{\text{reg}} \\ \vdots \end{Bmatrix} = \begin{Bmatrix} \vdots \\ f_{\Delta T} \\ \vdots \end{Bmatrix} + \begin{bmatrix} \mathbf{P}_N \end{bmatrix} \begin{Bmatrix} \mathbf{N} \\ \mathbf{M} \end{Bmatrix} - \begin{bmatrix} \mathbf{P}_p \end{bmatrix} \begin{Bmatrix} \vdots \\ \boldsymbol{\varepsilon}_{\text{reg}}^p \\ \vdots \end{Bmatrix} \quad (19)$$

where ${}_0\boldsymbol{\varepsilon}$ and $\boldsymbol{\kappa}$ are the midplane strain and curvature, respectively, $\boldsymbol{\sigma}_{\text{reg}}$ is the region stresses for each ply, $f_{\Delta T}$ is the thermal component, \mathbf{N} and \mathbf{M} are the applied forces and

moments, and ε_{reg}^p represents the region plastic strains in each ply. The matrices, P , P_N , and P_p relate the various quantities according to the model [26-27].

Since all the fibers do not debond at exactly the same time when the interface maximum stress is reached, a statistical model must be used to predict the behavior of the interface in the micromechanics model [27]. The model assumes that debonded interfaces carry zero stress and that the interfacial stresses can be represented by a single Gaussian distribution. From this assumption, the average interfacial displacement is determined to be:

$$\delta_{I,avg} = C_u \left\{ \frac{S}{\sqrt{2\pi}} \exp \left[-\frac{(\sigma_{I,ult} - \sigma_m)^2}{2S^2} \right] + \frac{\sigma_m}{2} \left[1 - \operatorname{erf} \left(\frac{\sigma_{I,ult} - \sigma_m}{S\sqrt{2}} \right) \right] \right\} \quad (20)$$

where σ_m is the mean interfacial stress, $\sigma_{I,ult}$ is the stress at which all interfaces have failed, S is the standard deviation of the stress distribution, and erf is the error function.

Equation 20 forms the basis of the interfacial damage model. The value $\delta_{I,avg}$ divided by the fiber diameter yields an effective way to measure the average interfacial damage in the composite as determined by the micromechanics model. For the purposes of this study, a $\delta_{I,avg}$ /fiber diameter ratio of .04 is considered to be fully debonded.

2.3 Fatigue Life Models

Fatigue in any material, homogeneous or not, is often hard to predict. Over multiple load cycles, surface or interior flaws may dramatically affect the behavior of the material under load. This is especially true for either very high or very low applied loads. Fatigue behavior in composites is even harder to predict due to the presence of an imbedded flaw: the interface between the fiber and matrix materials. The interfacial

reactions to loading makes accurate modeling of fatigue behavior even more difficult. This difficulty is somewhat lessened when modeling unidirectional composites with the fiber axis parallel to the applied load, because interfacial failure no longer plays a major role.

Despite the apparent difficulties in modeling composite fatigue, many researchers have attempted with varying degrees of success to model fatigue in titanium matrix composites. Several have proposed models based on statistical considerations of the behavior exhibited by one or more constituents of the composite [28-30]. Other researchers have developed empirical functions to model fatigue based on the behavior of the components [6, 31]. Still other researchers have developed a model based on the stress redistribution between layers of the composite as the various layers reach their maximum stress [32]. In this latter approach, the fatigue of a composite containing 0° plies is assumed to be controlled primarily by the behavior of the 0° plies [32].

The present effort modifies one of the empirical models by using micromechanics. This model was developed by Nicholas, et. al. in a series of publications [5-8, 33]. The basis of the model for isothermal fatigue is shown in Equation (21):

$$\frac{1}{N} = \frac{1}{N_c} + \frac{1}{N_t} \quad (21)$$

where N is the cycles to failure of the composite, N_c is the cycles to failure due to cyclic effects, and N_t is the cycles to failure due to time dependent conditions. N_c and N_t are further expanded as follows for isothermal fatigue:

$$N_c = A(\Delta\sigma)^{-m} \quad (22)$$

$$\frac{1}{N_t} = \frac{1}{f \sigma_{\max} (1-R)} \int_{R\sigma_{\max}}^{\sigma_{\max}} \frac{d\sigma}{t_c(\sigma)} \quad (23)$$

$$t_c = B\sigma^{-n} \quad (24)$$

where f is frequency, R is the stress ratio, $\Delta\sigma$ is the applied stress range, and t_c is the time-to-failure under constant stress. All other parameters in the Equations (22-24) are empirical constants. The model was later modified [7] by adding an interaction term to better match experimental data:

$$\frac{1}{N} = \frac{1}{N_c} + \frac{1}{N_t} + \frac{1}{N_i} \quad (25)$$

$$N_i = C\sqrt{N_c N_t} \quad (26)$$

where N_i is the interaction term and C is another empirical constant. In this model, the empirical parameters are functions of temperature.

A nonlinear variation of this model is presented in reference [5] for isothermal fatigue. In this model, the interaction term is eliminated and the time dependent term is replaced by a nonlinear term:

$$\frac{N}{N_c} + \left(\frac{N}{N_t}\right)^5 = 1 \quad (27)$$

The cyclic damage term is further modified as follows:

$$N_c = A(\Delta\sigma_{\text{eff}})^{-m} \quad (28)$$

$$\Delta\sigma_{\text{eff}} = \sigma_{\max}(1-R)^p \quad (29)$$

where R is the stress ratio and p is an additional empirical constant. For $p=1$, $\Delta\sigma$ is the governing term. For $p=0$, σ_{\max} is the governing term. The empirical constants in this

model are not the same as the constants for the linear damage accumulation model discussed above.

A thermomechanical fatigue prediction model has been developed which was also based on the isothermal nonlinear model described by Equation (27) [5]. In this model, the cyclic term is further broken down into terms governed by the fiber and matrix stresses as follows:

$$\frac{1}{N_c} = \frac{1}{N_f} + \frac{1}{N_m} \quad (30)$$

where N_f is the fiber stress based term, and N_m is the matrix stress based term. N_f and N_m are defined as follows:

$$N_f = 10^{N_0 \left(1 - \frac{\sigma_{f,\max}(1-R_f)^p}{\sigma_0} \right)} \quad (31)$$

$$N_m = B_m (\Delta\sigma_m)^{-n_m} \quad (32)$$

where $\sigma_{f,\max}$ is maximum stress in the fiber, R_f is the stress ratio of the fiber, $\Delta\sigma_m$ is the stress range in the matrix, and N_0 , σ_0 , p , B_m , n_m are empirical constants. σ_m and σ_f must be determined by a micromechanics model of the composite. After some assumptions on the nature of the temperature dependency of B and n in Equation (24), N_t is redefined for thermomechanical fatigue as:

$$\frac{1}{N_t} = \frac{\sigma_{\max}^n}{fB(1-R)^2} F \quad (33)$$

$$F = \begin{cases} \frac{1}{n+2} - \frac{R}{n+1} & \text{for in - phase TMF} \\ \frac{1}{n+1} - \frac{1}{n+2} & \text{for out - of - phase TMF} \end{cases} \quad (34)$$

where f , B , n , R are as defined in Equations (23) and (24). F produces very accurate results for $n > 2$ and $R = 0.1$ [5]. Once again, the empirical parameters in this model are not necessarily the same as the parameters developed for the other two models.

An earlier variation of the thermomechanical fatigue model does not use a time dependent term [8]. Thus the cycles to failure of the composite based on the micromechanic stresses is given as:

$$\frac{1}{N} = \frac{1}{N_f} + \frac{1}{N_m} \quad (35)$$

$$N_f = 10^{N_0 \left(1 - \frac{\sigma_{\max}}{\sigma_0} \right)} \quad (36)$$

$$N_m = B(\Delta\sigma_m)^{-n} \quad (37)$$

where all parameters are as defined previously with one exception: σ_0 in this formulation represents the fiber stress when the laminate is subjected to a static load at its ultimate tensile strength. This model yields another set of empirical constants.

A common characteristic of all of the above models is the inability to predict the behavior of the composite under varying loading conditions using just one model with one set of constants. The present effort attempts to eliminate the time dependent terms by allowing the micromechanic model to account for time dependent phenomena. The primary equation used in the present method is Equation (35). The fiber and matrix terms

are defined by Equations (31) and (32).

2.4 Experimental Work

Most of the experimental data used for the present effort were generated previously by a variety of agencies including AFIT, Wright Laboratories, and NASA. Stress-strain data for titanium 15-3 at varying strain rates and elevated temperatures (482+) were generated by NASA's Langley Research Center [3]. Titanium 15-3's elastic properties for temperatures up to 650°C were also generated by researchers at NASA Langley [34]. Thus, only data for temperatures under 482°C were required to be generated by this study to characterize this alloy. The Air Force Wright Laboratories Materials Directorate has already tested and characterized titanium β 21s using the Bodner-Partom with directional hardening model [35].

Metal matrix composites using titanium β 21s or titanium 15-3 as the matrix have been extensively tested at a variety of research institutions under isothermal and thermomechanical fatigue loading. Table 1 shows the composite layups, load cases, and references available to the present study for titanium β 21s based systems, and Table 2 contains the same information for titanium 15-3 based systems. Unless otherwise noted, the load ratio, R , is equal to 0.1 in all cases.

Table 1. SCS-6/Ti-β21s Fatigue Data

Layup	Iso/TMF	Temp (°C)	Freq (Hz)	Ref	Notes
[0/90] _s	Iso	650, 815	0.01, 0.1, 1, 200	5	
[0/90] _s	TMF	150-650	0.00556, 0.000556	5	In Phase & Out of Phase
[0] ₄	TMF	150-650	0.00556	36	In Phase & Out of Phase
[0/±45/90] _s	TMF	150-650	0.00556	36	In Phase & Out of Phase

Table 2. SCS-6/Ti-15-3 Fatigue Data

Layup	Iso/TMF	Temp (°C)	Freq (Hz)	Ref	Notes
[0]8	Iso	25	1, 10	37-39	R = 0
		427	0.33	40	
		650	10	41	
[0]8	TMF	93-538	0.0056	40	In/Out of Phase, R=0
[90]8	Iso	25	1	37, 38	R = 0
		427	.33, .0083	40	
[90]8	TMF	200-427	0.0083	40	In/Out of Phase, R=0
[0/90] _s	Iso	25	10	37	
		427	2, 0.02	42	
		650	10	41	
[0/90] _s	TMF	149-427	0.02	42	In/Out of Phase
[0/±45/90] _s	Iso	25	10	37	
		427	0.02	43	
		650	10	41	
[0/±45/90] _s	TMF	149-427	0.02	43	
[±45]2s	Iso	427	0.02	44	
[±45]2s	TMF	149-427	0.02	44	

III. Methodology

Titanium based metal matrix composites have been extensively examined recently for use in high performance aerospace applications at elevated temperatures. Because of the relatively high cost of titanium matrix composites, it is highly desirable to develop an accurate model to predict the behavior of these materials under a variety of load cases. This effort uses two different approaches to predict fatigue life. One modifies an existing model [5-8] by replacing the time dependent terms with information from a micromechanics model [4]. The other creates a new model based on the fatigue behavior of the homogeneous matrix material and the micromechanical stresses [4].

Since stress strain behavior of titanium is dependent on the loading rate, both of these approaches require a good understanding of the viscoplastic behavior of the matrix material. The modified Bodner-Partom unified viscoplastic theory [1, 2, 16] is used to characterize the titanium matrix; thus, requiring the development of a set of material dependent constants. Constant strain rate tensile tests are required to provide experimental data to calculate these parameters. Other researchers have done this and developed the constants for titanium β 21s [35]. However, this has not yet been accomplished for the titanium 15-3 alloy using the Bodner-Partom theory with directional hardening.

3.1 Viscoplastic Characterization of Ti-15-3

Characterizing the titanium 15-3 matrix required two distinct tasks. The first was to select and perform experiments at appropriate temperatures to complement the data already available in the literature [3]. The second task was to determine what constants in

the Bodner-Partom model will best predict the experimental curves.

3.1.1 Experimental Procedure

The material used for the experimental portion of the present study was titanium 15-3. The test panel used was fabricated using the same procedure as for the composite form. The matrix layers are thin, cold-rolled sheets of titanium. Usually, the fibers and titanium sheets are arranged in the desired layup and then joined by hot isostatic pressing [3]. This process was used on the titanium sheets without the fibers to produce a homogeneous panel of titanium. The panel was then cut into individual rectangular samples, 152.4 mm x 12.7 mm x 1.84 mm in size. A total of 5 tests were accomplished: 1 at room temperature and a strain rate of 0.001/s, 2 each at 315°C and 427°C with strain rates of 0.01/s and 0.0001/s.

The tests were conducted on a servo-hydraulic test stand (Material Test System 808) equipped with a 10 kip load cell and programmed for constant strain rate. The data collection was accomplished on a Zenith 248 computer with the AFIT developed program, BETASTAT. After receiving test parameters from the user, this program records the data from the test stand into ASCII files. In all of the tests, axial strain was measured with a 0.5 inch gage length, high temperature, quartz rod extensometer (MTS model 632.50b-04). For the room temperature test, a transverse strain gage was also mounted on the sample to measure off-axis strain. For the elevated temperature tests, a thermocouple was mounted on each side of the sample to control temperature generated by parabolic lamps. The lamps were mounted on the test stand to heat each side of the specimen. The thermal

strain was measured after heating.

3.1.2 Constant Determination

Determination of the Bodner-Partom constants was accomplished on a Micro Technix 486 DX computer using MathCad 5.0+ (MathSoft). The viscoplastic algorithm developed by Robertson [4] was translated from FORTRAN to Borland C++ version 4.0. It was also reformulated from uniaxial load control to uniaxial strain control. The C++ program was then linked to MathCad 5.0+ as the function *bodpart(M)*, where the argument M is a matrix of the constants and strain control information. The C++ code used to create *bodpart(M)* is located in Appendix A.

Since the Bodner-Partom theory does not result in a closed form solution, an iterative algorithm is required to determine the level of stress at a given level of strain. The sequence of steps used to compute the stress for a single uniaxial strain-time increment is given below.

- (i) Initialize the stress and elastic strain rate at interval $t_p = t_{p-1} + \Delta t$ by assuming that the response is purely elastic:

$$\sigma_p = \sigma_{p-1} + E\dot{\epsilon}\Delta t \quad (38)$$

$$\dot{\epsilon}^I = 0 \quad (39)$$

- (ii) Calculate the inelastic strain rate resulting from the directional and isotropic hardening resulting from the current values of σ_p and $\dot{\epsilon}^I$ using the Bodner-Partom theory:

$$\dot{W}_p = \sigma_p \dot{\epsilon}^I \quad (40)$$

$$Q = -m_1 \dot{W}_p - \frac{a_1 Z_1^{(1-r_1)} (Z_p^I - Z_2)^{r_1}}{Z_p^I} \quad (41)$$

$$dZ^I = \frac{m_1 Z_3 \dot{W}_p - Q Z_{p-1}^I}{\frac{1}{\Delta t} - Q} \quad (42)$$

$$Z_p^I = Z_{p-1}^I + dZ^I \quad (43)$$

$$Q_2 = -m_2 \dot{W}_p - a_2 \left(\frac{Z_p^D}{Z_1} \right)^{(r_2-1)} \quad (44)$$

$$dZ^D = \frac{m_2 Z_3 \dot{W}_p + Q_2 Z_{p-1}^D}{\frac{1}{\Delta t} - Q_2} \quad (45)$$

$$Z_p^D = Z_{p-1}^D + dZ^D \quad (46)$$

$$\dot{\epsilon}_{cal}^I = \frac{2D_0}{\sqrt{3}} \exp \left[-\frac{1}{2} \left(\frac{Z_p^I + Z_p^D}{\sigma_p} \right)^{2n} \right] \quad (47)$$

(iii) Determine the change in the effective inelastic strain rate from the calculated value in step (2) and the value used for the previous iteration:

$$\delta \dot{\epsilon}^I = \dot{\epsilon}_{cal}^I - \dot{\epsilon}^I \quad (48)$$

(iv) Calculate the scaling ratio, R, by:

$$R = \begin{cases} \frac{-\delta \dot{\epsilon}^I}{\delta \dot{\epsilon}^I - k \delta \dot{\epsilon}_{max}} & \text{for } \delta \dot{\epsilon}^I < 0 \\ \frac{\delta \dot{\epsilon}^I}{\delta \dot{\epsilon}^I + k \delta \dot{\epsilon}_{max}} & \text{for } \delta \dot{\epsilon}^I \geq 0 \end{cases} \quad (49)$$

where k is a user-supplied constant (usually between 2 and 30) to control

convergence stability and $\delta\dot{\epsilon}_{\max}$ is the maximum change in strain rate between iterations and is given by:

$$\delta\dot{\epsilon}_{\max} = \sqrt{\frac{2}{3} \left[\dot{\epsilon}^2 + 2(v\dot{\epsilon})^2 \right]} \quad (50)$$

(v) Update the inelastic strain rate with the new scaling ratio:

$$\dot{\epsilon}^I = \dot{\epsilon}^I + R\delta\dot{\epsilon}_{\max} \quad (51)$$

(vi) Use the new inelastic strain rate to calculate the stress for the current iteration:

$$\sigma_p = \sigma_{p-1} + E(\dot{\epsilon} - \dot{\epsilon}^I)\Delta t \quad (52)$$

(vii) Check convergence. If:

$$\frac{\delta\dot{\epsilon}^I}{\delta\dot{\epsilon}_{\max}} < 0.001 \quad (53)$$

then use the value of σ_p calculated in step (vi) and proceed to step (i) with the next time step. If not, return to step (ii), using the new values of stress and inelastic strain rate.

Once the Bodner-Partom algorithm was imbedded in MathCad, the experimental data were imported and the two curves were compared. The constants were then varied until a good match between the experimental and analytic curves was achieved. The constants were assumed to be functions of temperature. Therefore, this was accomplished at each temperature and strain rate. The constants were allowed to differ between temperatures, but not between strain rates.

3.2 Embedding Micromechanics into Existing Model

In the first phase of the present study, the viscoplastic Bodner-Partom constants for titanium 15-3 were determined for later use in a micromechanics model. The second phase of the present effort employs the micromechanics to eliminate the separate time-dependent terms in an existing fatigue life theory [5-8] previously discussed in section 2.3. The removal of the time-dependent terms from this model leaves the following 3 equations:

$$\frac{1}{N} = \frac{1}{N_m} + \frac{1}{N_f} \quad (54)$$

$$N_f = 10^{N_0 \left(1 - \frac{\sigma_{f,\max}(1-R)^p}{\sigma_0} \right)} \quad (55)$$

$$N_m = B_m (\Delta \sigma_m)^{-n_m} \quad (56)$$

where $\sigma_{f,\max}$ and σ_m are the microstresses in the fiber and matrix respectively, R is the stress ratio, and N_0 , σ_0 , p , B_m , and n_m are empirical material constants. Unlike in earlier versions of this model [8], σ_0 does not have a defined physical significance in this study. It is used here as an additional empirical constant.

The micromechanics program, *LISOL* [4], was used with Neu's Bodner-Partom constants [35] for titanium $\beta 21s$ and the Bodner-Partom constants developed for titanium 15-3 in this effort to determine the microstresses in the composite. The SCS-6/Ti- $\beta 21s$ composite was emphasized in this phase, because fatigue life data at varying frequencies are readily available [5], allowing comparison's between different load rates. In each case,

the maximum fiber stress, usually in the 0° ply, and the maximum matrix stress, usually in region 2 of the 0° ply, were used. The values were taken from the 20th cycle to allow the viscoplastic effects time to stabilize. The microstresses from *LISOL* were loaded into MathCad and curve-fitted, using a second or third degree polynomial, to provide continuous functions with the applied composite stress as the argument. The functions for $\sigma_{f,max}$ and $\Delta\sigma_m$ were subsequently inserted into the Equations (54-56) above and compared to experimental data. The constants were then varied until a good curve fit was achieved.

3.3 Constituent Behavior Based Model

This model was developed by assuming linear damage accumulation behavior, and that the matrix material in a composite behaves under fatigue similarly to the homogeneous matrix material. This theory was developed for unidirectional or cross-ply laminates composed of 0° and/or 90° plies where the fatigue life of the 0° plies is given as:

$$\frac{1}{N} = \frac{1}{N_m} + \frac{1}{N_f} \quad (57)$$

and the fatigue life of the 90° plies is given as:

$$\frac{1}{N} = \frac{1}{N_m} + \frac{1}{N_f} + \frac{1}{N_I} \quad (58)$$

where N_I is a term driven by the fiber-matrix interface damage.

The behavior of the matrix material is shown in the following equation:

$$N_m = B_m \sigma^{-n} \quad (59)$$

where σ is the maximum applied stress, and B_m and n are material constants. The stress ratio, R , for the development of this theory was 0.1. The fibers are assumed to behave the same as in Equation (55) from Section 3.2. The behavior function for the interface in the

90° ply was developed by fitting a curve to data retrieved from *LISOL* denoting approximate cycle count to complete interfacial failure. The resulting curve was then modified to account for the propagation of the interfacial cracks into the matrix material.

Experimental data from three tests [38] were required to develop this model. Fatigue data for titanium 15-3 were needed to determine the material constants for N_m , fatigue data for a 0° laminate were required to determine the constants for N_f , and, finally, data for 90° plies were used to determine the constants for N_i . In each case, microstresses from *LISOL* were expressed as continuous functions of the overall applied stress. These functions were then used as the input into Equations (57), (58), (59), and (55) to determine the material constants which best matched the experimental data. Once the constants required to predict lamina behavior were determined, *LISOL* was used to determine the level of stress seen by each ply of a cross-ply laminate. These stresses were then used to develop life predictions for each ply, and this information was used to determine the fatigue life of a cross-ply composite. Several combination techniques were explored; including linear damage accumulation, geometric averaging, and use of the 0° ply microstresses.

IV. Results and Discussion

Titanium based metal matrix composites have many mechanical and thermal properties which make them desirable for use in high performance aerospace applications. Their cost, however, makes it even more desirable to be able to predict their behavior under load without expending material to do so. To understand the behavior of the composite, it is necessary to understand the micromechanical behavior of each of the constituents in the composite. The fiber material, silicon carbide, can be accurately depicted as a brittle linear elastic material. The matrix material, titanium, however, requires a more complex viscoplastic theory to accurately model its behavior. The model chosen for the present effort is the Bodner-Partom theory with directional hardening [1, 2, 16].

Since the alloys in question, titanium β 21s and 15-3, are relatively new, they must be properly characterized before use in the micromechanics model. This has been accomplished for the β 21s alloy [35] using the desired theory. Characterization using Bodner Partom with directional hardening has not been done for the 15-3 alloy, although previous efforts have characterized titanium 15-3 using an earlier variant [3]. The first phase of the study characterizes titanium 15-3. It then puts the new material parameters into a micromechanics model to predict the behavior of titanium 15-3 matrix composites.

The second phase of the present effort uses the microstress predictions from the micromechanics to replace the independent temporal terms in a previously developed fatigue model [5-8]. This model is used to predict behavior of the composite under isothermal thermomechanical fatigue at various temperatures. The final phase of the

present effort attempts to create a new fatigue behavior model based on the micromechanics and constituent fatigue behavior.

4.1 Characterization of Titanium 15-3

Titanium 15-3 was characterized using the Bodner-Partom unified viscoplastic theory with directional hardening. Experimental data for temperatures of 482°C and above were available from other sources [3], but data for temperatures under 482°C had to be developed as part of this effort. Once the data required were obtained, the material constants were obtained through iterative curve-fitting in MathCad.

4.1.1 Experimental Results

Figures 2, 3, and 4 show the stress strain curves obtained by testing titanium 15-3 at constant strain rates at room temperature, 315°C, and 427°C, respectively. The strain rates are as indicated in each figure.

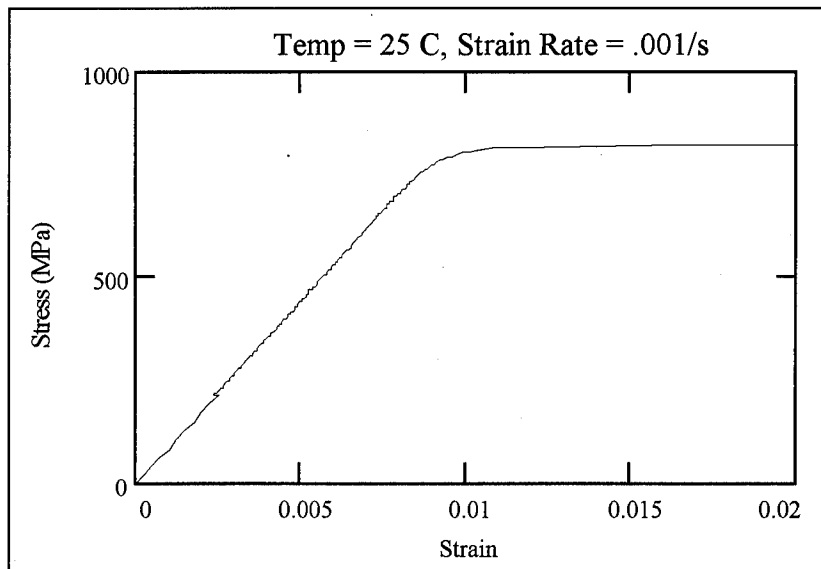


Figure 2. Ti-15-3, Room Temperature

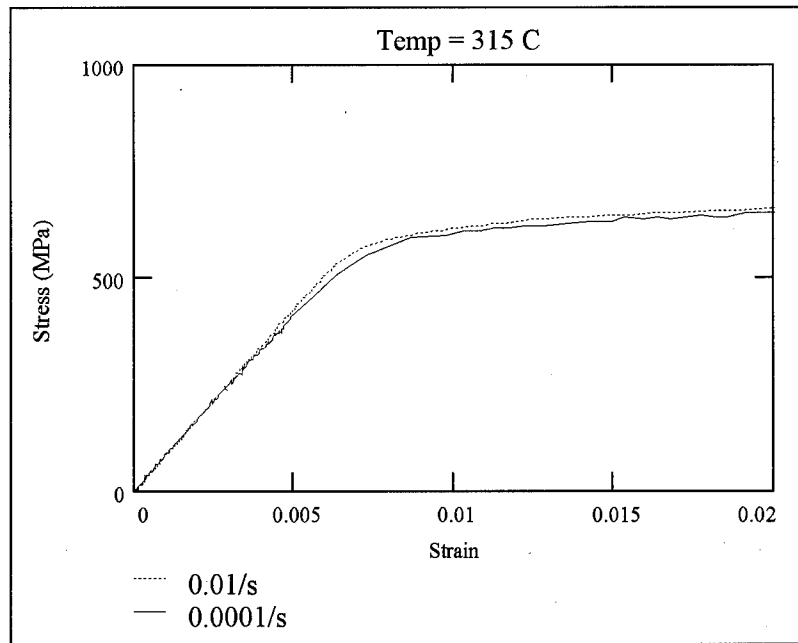


Figure 3. Ti-15-3, 315°C

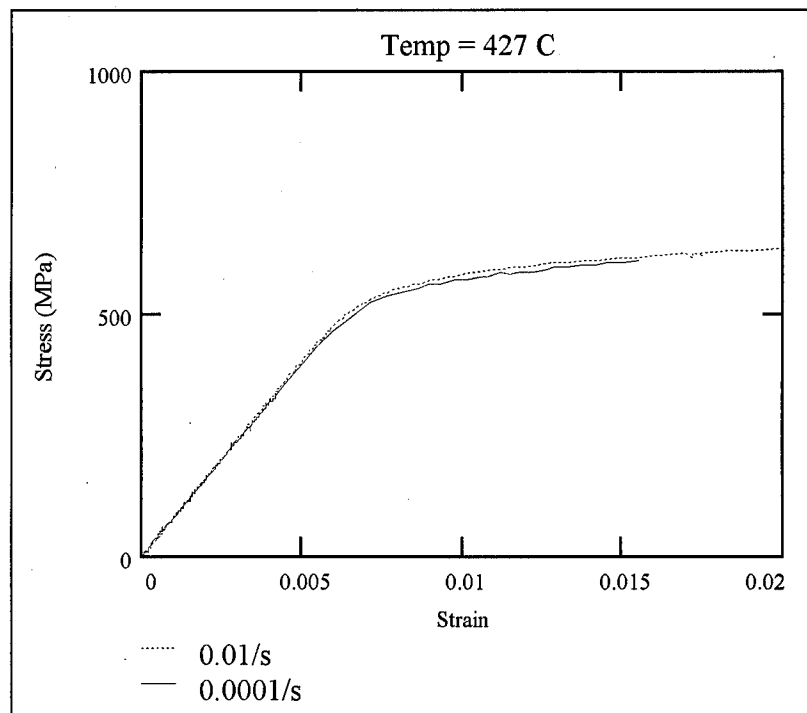


Figure 4. Ti-15-3, 427°C

Fracture was not reached in any of the five tests. The 0.0001/s curve at 427°C was cut short due to saturation of the memory available to collect the data. In both the 315°C and the 427°C tests, differences in strain rate did not make a significant impact. During the room temperature test, Poisson's ratio, ν , was also determined and is graphed versus axial strain in Figure 5:

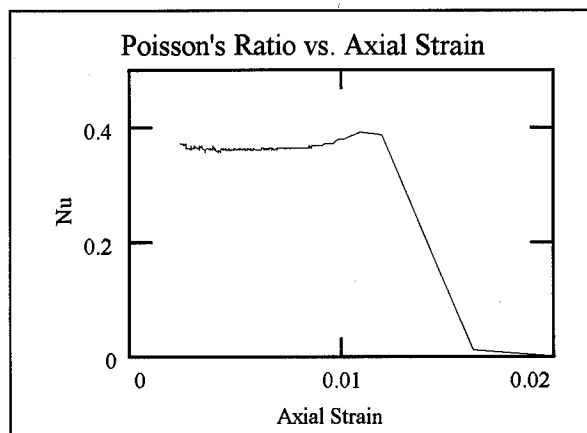


Figure 5. Poisson's Ratio for Ti-15-3

The values in the elastic region vary from about 0.355 to 0.365. This corresponds very well with the previously determined [34] value of 0.36 for titanium 15-3. The microstrain gage slipped as the material reached its yield point resulting in the transverse strain, and thus ν , dropping down to 0 in the above graph.

The thermal expansion coefficient for titanium 15-3, α , was determined at 315°C and 427°C with 25°C as a reference temperature by measuring the thermal strain before loading occurred. At 315°C, α was calculated to be 11.1×10^{-6} m/m/°C, and at 427°C, α was determined to be 14.7×10^{-6} m/m/°C. Both of these values are significantly higher than those previously determined by other researchers [34] who reported values of about

9×10^{-6} m/m/°C in this temperature range. Because the previously determined values have been generally accepted by the research community, they were used in the present effort.

4.1.2 Viscoplastic Characterization

After the stress strain data were acquired from the experiments and previous research [3], they were inputted and plotted in MathCad. The viscoplastic algorithm was created and linked to MathCad via the function *bodpart*. The initial guess of the Bodner-Partom constants was taken from reference [23]. These previous constants were determined from an incomplete set of experimental data and were found to predict the elastic behavior and the yield point with some degree of accuracy, but did a poor job of predicting plastic hardening.

After several iterations, the Bodner-Partom constants for titanium 15-3 were determined to be as follows:

Temperature dependent constants:

Table 3. Temp. Dependent Bodner-Partom Constants

Temp (°C)	E (GPa)	Z ₂ (MPa)	Z ₃ (MPa)	n	a ₁ = a ₂ (sec ⁻¹)	m ₂ (MPa ⁻¹)
25	86.3	1200	250	4.5	10 ⁻⁸	.005
315	80.4	1070	454	2.9	4.4x10 ⁻⁶	.04
427	77.5	1020	550	2.7	10 ⁻⁵	.05
482	72.2	850	1100	1.6	1	5
566	64.4	750	2400	1.05	2.5	15
650	53.0	650	3000	0.9	3	20

Temperature independent constants:

$$D_0 = 10^4 \text{ s}^{-1} \quad Z_1 = 1300 \text{ MPa} \quad r_1 = 3 \quad r_2 = 3 \quad m_1 = 0 \text{ Mpa}^{-1}$$

Figures 6-10 show the experimental behavior of titanium 15-3, the behavior predicted by the previous constants, and the behavior predicted by the new constants at the six temperatures in Table 1.

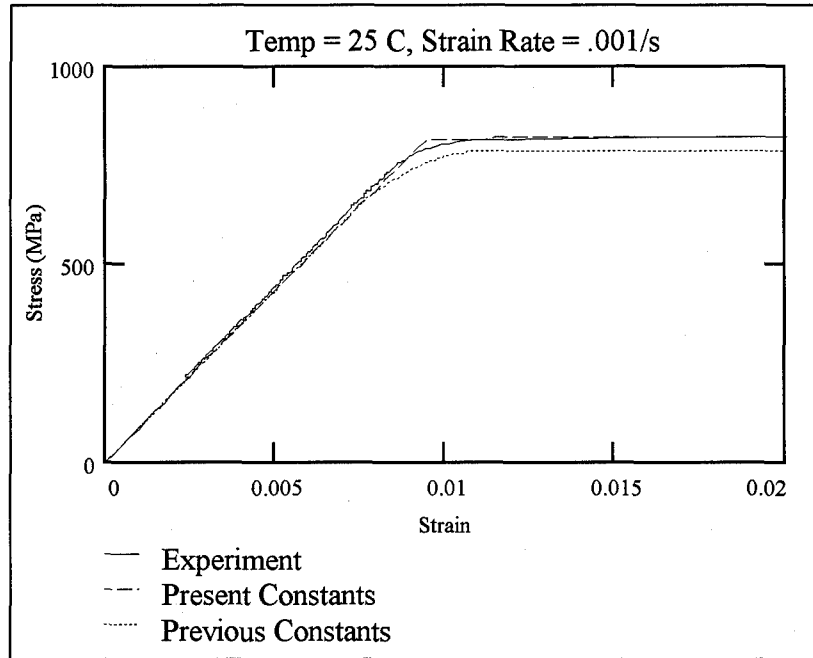


Figure 6. Ti-15-3, Room Temp, .001/s

As Figure 6 shows, both the constants from previous work and the ones determined in the present effort correlate well with the experimental results. The present method is slightly closer to predicting the actual behavior. As temperature increases, the difference between the old and new constants is more pronounced.

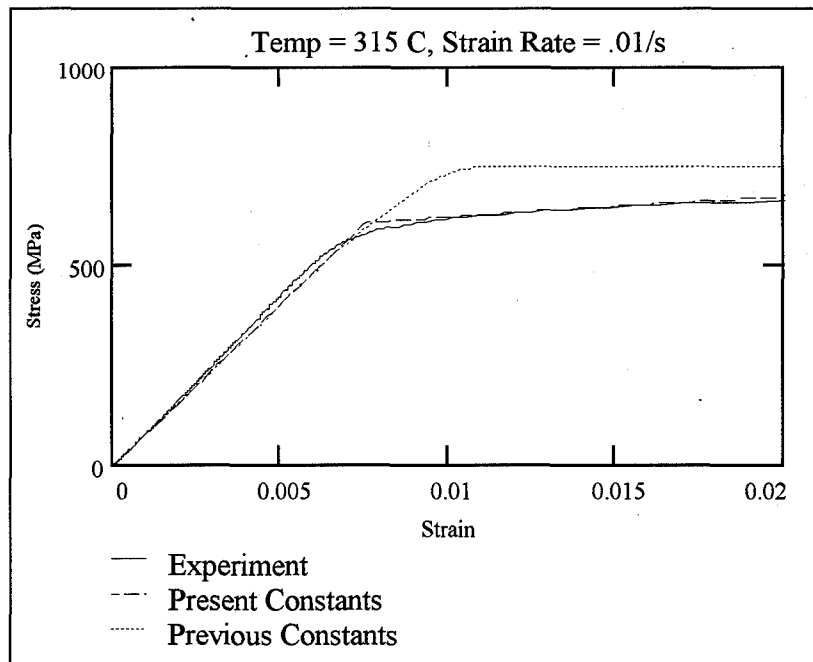


Figure 7. Ti-15-3, 315°C, .01/s

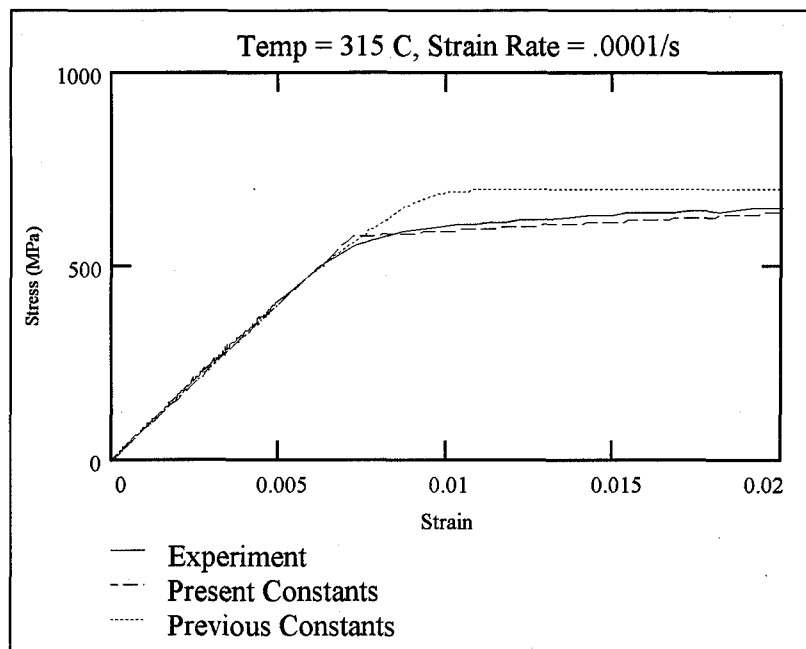


Figure 8. Ti-15-3, 315°C, .0001/s

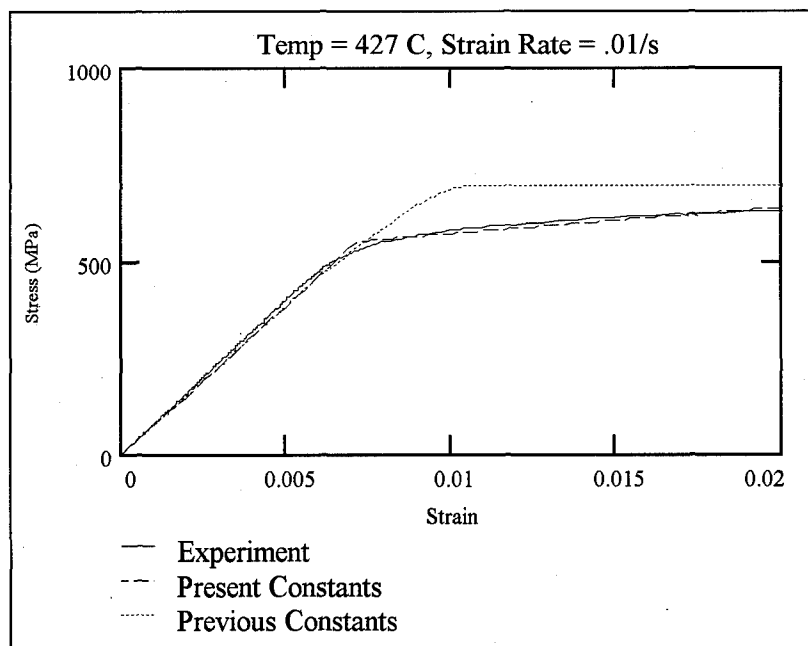


Figure 9. Ti-15-3, 427°C, .01/s

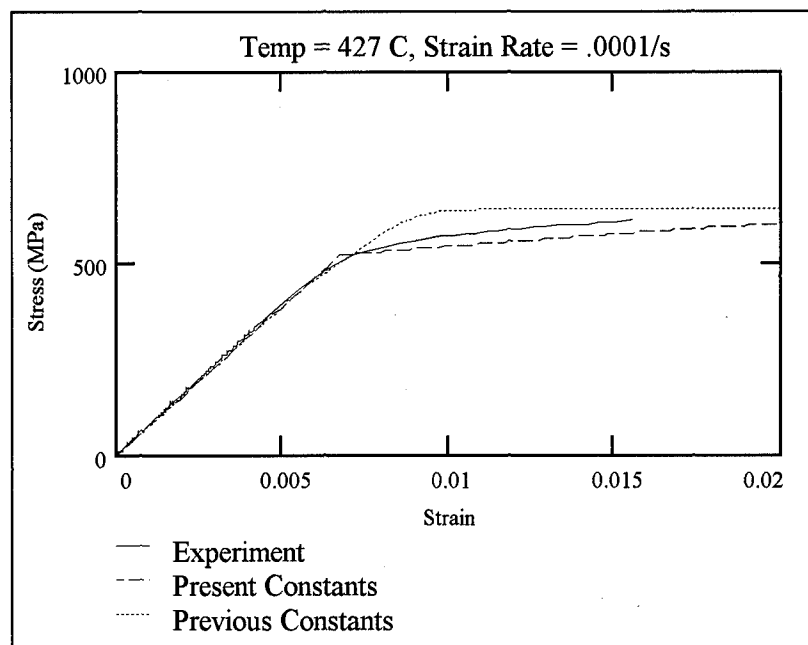


Figure 10. Ti-15-3, 427°C, .0001/s

Experimental data from other researchers [3] were used to generate the constants for temperatures above 427°C. At these higher temperatures, strain rate became more of a factor. Figures 11-16 show the stress strain curves for 482°C, 566°C, and 649°C. Each of the graphs contains the experimental stress strain curve, the curve predicted using the previously developed constants, and the curve predicted by the new constants.

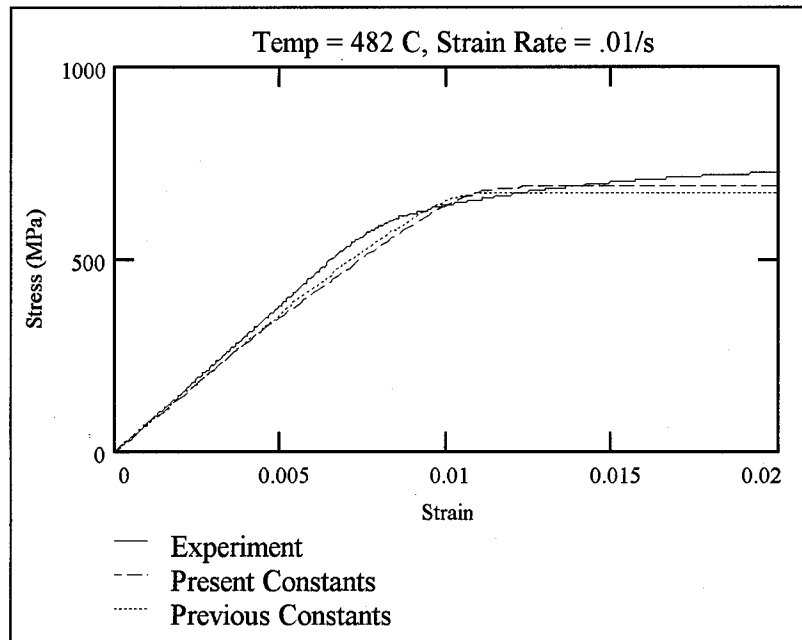


Figure 11. Ti-15-3, 482°C, .01/s

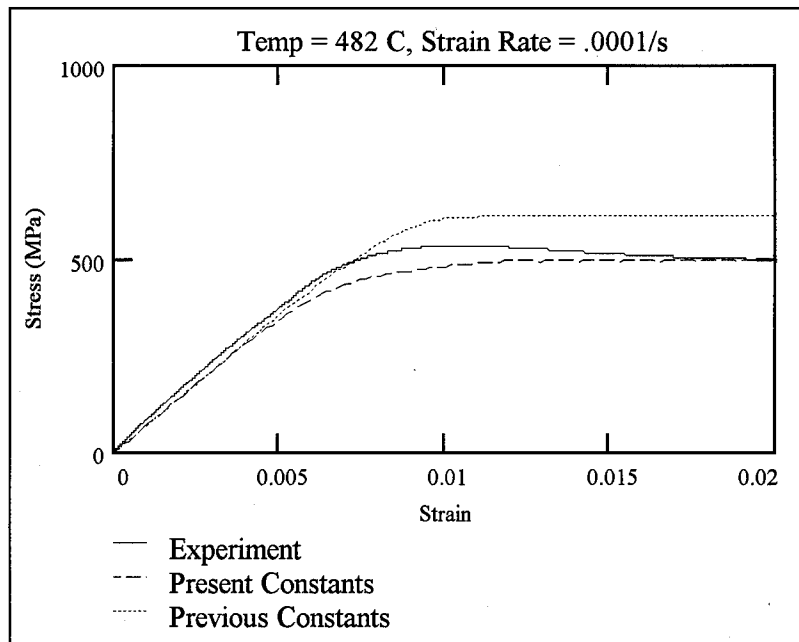


Figure 12. Ti-15-3, 482°C, .0001/s

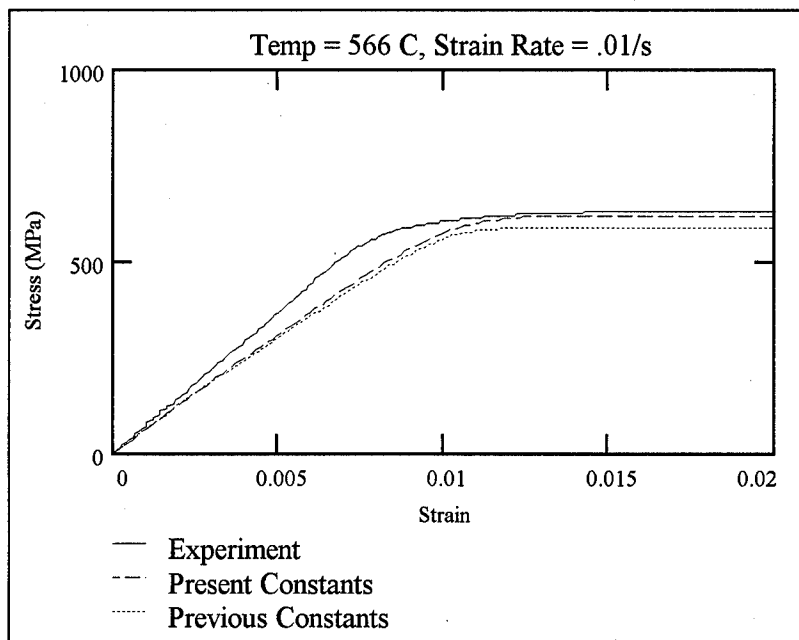


Figure 13. Ti-15-3, 566°C, .01/s

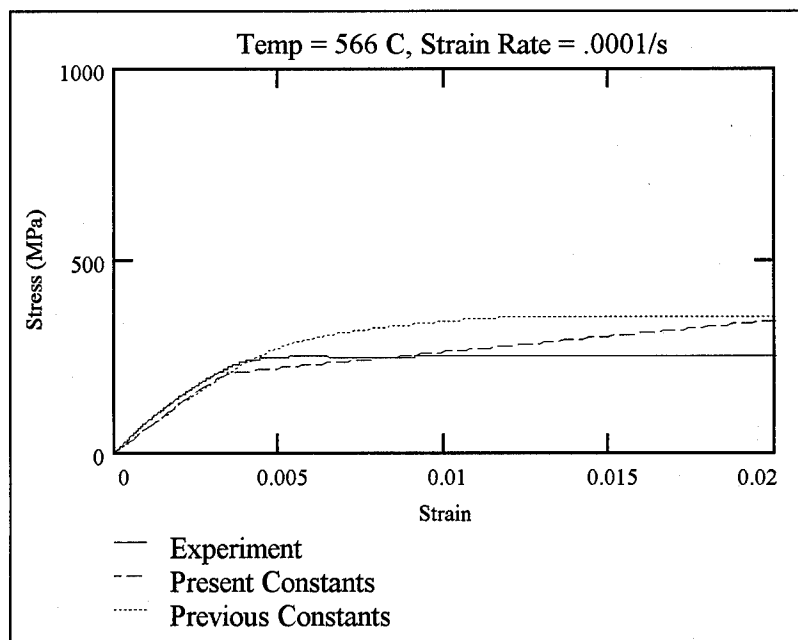


Figure 14. Ti-15-3, 566°C, .0001/s

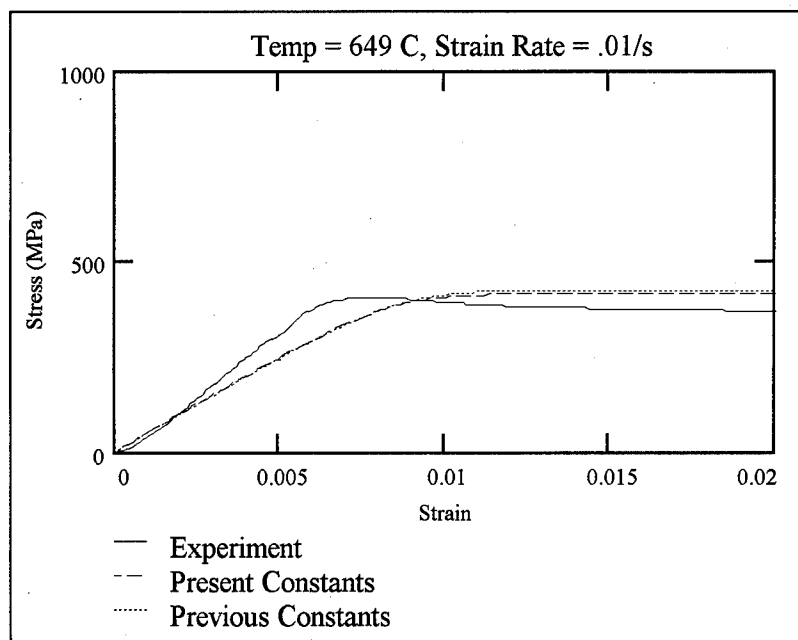


Figure 15. Ti-15-3, 649°C, .01/s

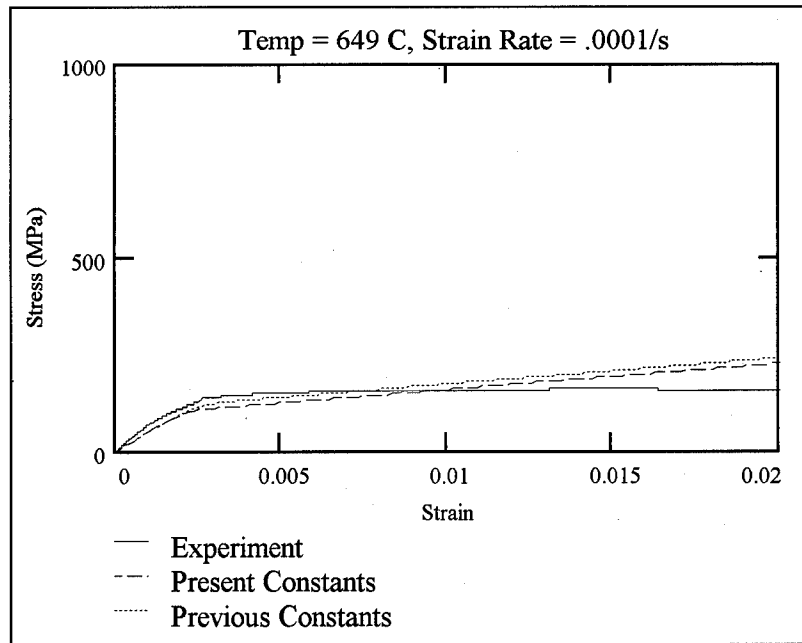


Figure 16. Ti-15-3, 649°C, .0001/s

As can be seen in the last 6 figures, titanium 15-3 behaves substantially different at temperatures above about 450°C than at temperatures below 450°C. Strain rate is much more important in establishing the shape of the stress strain curves for the higher temperatures. Additionally, the behavior after yield at the higher temperatures is nearly perfectly plastic. Since the previously used constants predict perfect plasticity at all temperatures, they perform nearly as well as the new constants at the higher temperatures. The new constants tend to overpredict plastic hardening at the slower strain rates, but do a good job of predicting the perfect plastic behavior at the high strain rates. Since the frequencies examined in the present effort tend to be greater than 1 hertz, greater emphasis was put on establishing a good curve fit at the higher strain rates. In no case,

were the viscoplastic constants allowed to vary between strain rates.

4.1.3 Micromechanics Application

Once viscoplastic characterization was accomplished, the new constants were installed into the micromechanics model, and the model was run to determine if the new constants improved on the predictive accuracy of the model for a laminate when compared to experimental data [44]. The angle ply layup ($[\pm 45]_s$) was used for this analysis since it is assumed that the matrix dominates the behavior of this particular laminate under load. The model was applied to two different load cases: monotonic loading up to 340 MPa and isothermal fatigue loading with a maximum stress of 300 MPa. Figure 17 shows the monotonic load case.

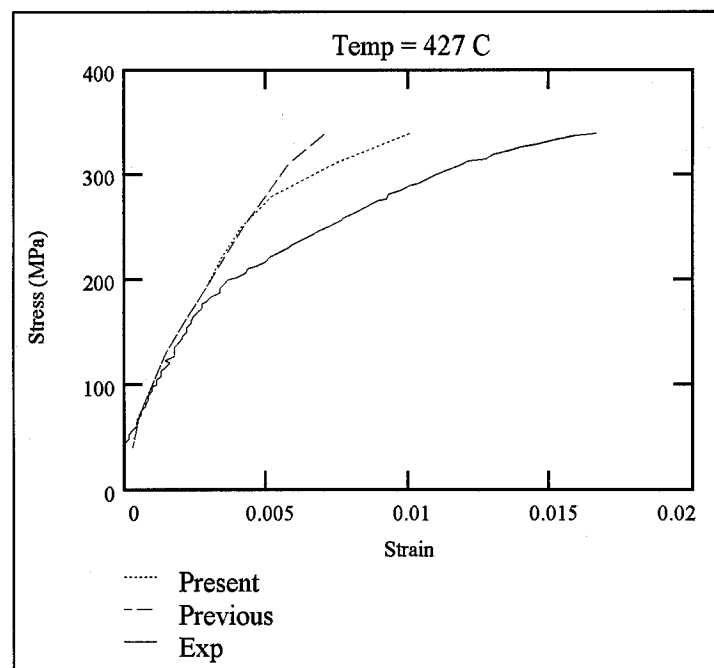


Figure 17. Angle Ply, Stress-Strain, 427°C

As Figure 17 shows, the new constants come closer to the actual stress strain behavior for an angle ply layup than do the old constants. The micromechanics model with either set of constants tends to over predict the strength of the laminate. A recent upgrade of the micromechanics model to include shear failure of the interface nearly eliminates this discrepancy [25]. However, this upgrade was not included in the present effort. The older version of the micromechanics does produce a reasonable prediction of the general shape of the stress strain curve.

Figure 18 shows the maximum and minimum strain during fatigue loading with a maximum stress of 300 MPa, a stress ratio of 0.1, and a cycle period of 24 seconds.

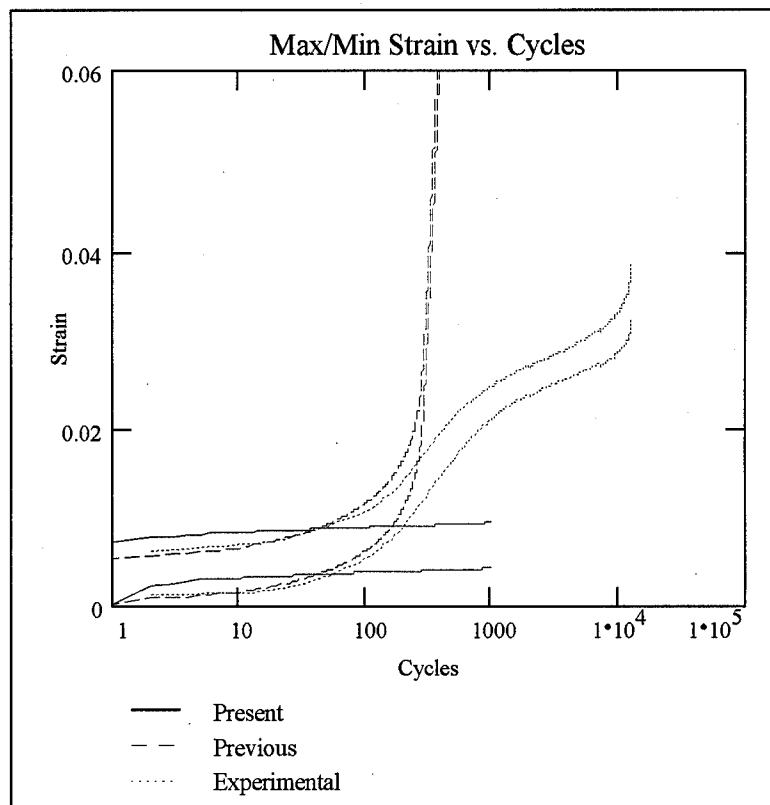


Figure 18. Angle Ply, Max-Min Strain History Under Isothermal Fatigue (Max Stress = 300 Mpa), 427°C

Under this loading condition, neither the old nor the new constants is completely accurate. The micromechanics model using the old constants does an excellent job for the first 100 or so cycles, but then, since the old constants do not account for plastic hardening, the model drastically over predicts the strain. The model with the present constants converges well, but does a poorer job during the low cycles and does not follow the experimental curve upwards for the higher cycles. This is probably due to the micromechanics model not accounting for the failure of fibers or matrix material over the cyclic loading.

4.1.4 Viscoplastic Discussion

Although a systematic approach to find the Bodner-Partom constants has been developed [18], it was not used, because it requires more experimental data than were available for the present study. Instead the parameters were developed empirically by comparing the curves generated by the theory to actual experimental curves. Some initial assumptions were made to facilitate this effort: (1) the viscoplastic behavior of titanium 15-3 is similar to that of titanium β 21s, (2) the viscoplastic constants are functions of temperature, but not of strain rate, and (3) the elastic constants (E and ν) are as determined previously at NASA Langley [34].

The first assumption allows the previously developed constants for the β 21s system [35] to be used as a reference for the behavior of the constants. For example, as temperature increases, Z_2 decreases and Z_3 increases for titanium β 21s. This same behavior was assumed in the present effort for titanium 15-3. The assumption of similar behavior between the β 21s and 15-3 alloys also allows the same constants (Z_1 , m_1 , r_1 , r_2 , D_0 , and ν) to be independent of temperature, sets a_1 equal to a_2 , and lets m_1 be equal to 0

(no isotropic hardening). The first and third assumptions are important, because they lower the number of constants which need to be determined at each temperature. The second assumption forces a single set of constants to address both high and low strain rates for each temperature. Others have allowed the constants to vary with strain rate [3] which make them more difficult to use in other applications. Even with these assumptions, there are still 35 constants to be determined with only 11 experimental data curves.

Since there are more constants than data curves, there are probably multiple sets of constants that can satisfactorily model the experimental data. The emphasis in this effort was to determine constants that would accurately predict the elastic behavior, the yield point, and the plastic hardening behavior at the faster strain rates. For example, the transition from elastic to plastic behavior was neglected in favor of plastic hardening behavior. Emphasis was also placed on the lower temperatures for two reasons: there is more fatigue data available for homogeneous titanium 15-3 at under 450°C and the stress strain curve shapes were less consistent at temperatures above 450°C.

The various constants affect the stress strain curve predictions in a variety of interactive ways. Z_1 and n primarily govern the yield point and the magnitude of the stress in the plastic region. An increase in one of these two constants shifts the plastic region of the stress strain curve higher. m_1 and a_1 combine to determine the level of plastic hardening. a_1 also affects the sensitivity of the stress strain curve to strain rate when Z_3 is greater than Z_2 . Figure 19 shows Z_2 and Z_3 plotted against temperature.

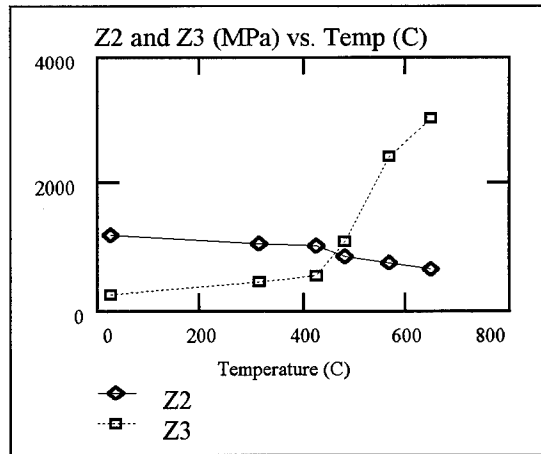


Figure 19. Ti-15-3, Z_2 & Z_3 vs Temperature

A transition occurs at about 450°C. Below this temperature, Z_2 is greater than Z_3 , and the stress strain behavior is relatively independent of strain rate. Above this temperature, Z_3 is greater, and the stress strain behavior is highly dependent on strain rate. r_2 and r_3 were not changed from the values determined in previous efforts for titanium 15-3 [45] or titanium β 21s [35]. A large number of other efforts assume that D_0 is equal to 10^4 sec^{-1} [3, 4, 35, 45], and that assumption is also made for the present effort.

Once the new constants were developed, they were put into the micromechanics model and tested for an angle ply layup. The new constants yielded discrepancies in both the monotonic load case and the fatigue load case. The discrepancies in the monotonic load case are probably due to the fact that the present micromechanics model only attempts to deal with the degradation of the interface in the normal direction to the fiber [4, 23]. Fiber failure, matrix failure, and interface shear failure are not accounted for at all. As a result, the micromechanics model can be expected to over predict the behavior of the composite. This is also true for the fatigue load case, which would explain the lack of

strain increases over the number of cycles. The difference between the result generated by the old constants and the result generated by the new is probably due to the lack of a smooth or gradual transition between the elastic and plastic regimes. The first problem must be addressed within the micromechanics model. The second must be addressed by either altering the viscoplastic model or the constants used in the model.

4.2 Linear Damage Accumulation Model

A previously developed fatigue model [5-8] was modified to use time dependent information from the viscoplastic micromechanics model, *LISOL* [4], instead of a separately defined term. The model as described in the literature [5-8] is discussed in detail in Section 2.3 of the present study. After removing the time dependent and interaction terms, N_t and N_i , respectively, the governing equations in this model become:

$$\frac{1}{N} = \frac{1}{N_f} + \frac{1}{N_m} \quad (60)$$

$$N_f = 10^{N_0 \left(1 - \frac{\sigma_{f,max}(1-R)^p}{\sigma_0} \right)} \quad (61)$$

$$N_m = B_m (\Delta\sigma_m)^{-n_m} \quad (62)$$

where σ_f and σ_m are the microstresses of the fiber and matrix respectively, R is the applied stress ratio, and the other parameters are empirical constants. This modified model was used first to examine the fatigue behavior of SCS-6/Ti- β 21s laminates and later to predict the fatigue life of SCS-6/Ti-15-3 composites. A single set of constants was developed for each material and maximum temperature.

4.2.1 SCS-6/Ti- β 21s Cross-Ply Isothermal Microstresses

The first step in developing a micromechanics based fatigue model was to use *LISOL* to determine the microstresses for isothermal fatigue at 650°C for a range of loads and frequencies. For the present study, the load ratio, R , was 0.1 for all tests and micromechanics analyses. In most cases, the microstresses from the 20th cycle were used to allow for the stabilization of the viscoplastic effects. In the remaining cases, the microstresses were taken from the cycle at which the fiber reached a plateau, indicating viscoplastic stabilization. Once several microstress data points were developed by *LISOL*, they were curve fitted to a polynomial using the Mathcad function *linfit*. This was accomplished to provide a continuous function for σ_f and σ_m in the model equations, allowing for easier curve fitting.

The frequencies researched in this effort were 0.01, 0.1, and 1 hertz. The maximum applied loads for each frequency ranged from 200 to 600 MPa. These values were chosen to match the experimental data available. In each case, the curve was stabilized fairly well within the 20th cycle. The differences between the 19th and 20th cycle fiber stresses for 0.01, 0.1, and 1 hertz were 0.5%, 0.8%, and 0.5%, respectively at a maximum applied stress of 200 MPa. Figure 20 shows the fiber stress plotted against the cycle count. Similar behavior was exhibited at higher stress levels with the maximum difference being 0.6%. At 400 and 500 MPa and 0.1 Hz, the fiber stresses plateaued before the cycle count reached 20. The plateau value was used instead of the value at the 20th cycles in these cases. The matrix microstresses also stabilized comparably to the

fiber stresses at the 20th cycle with a worst case difference between the 19th and 20th cycles of 1.7%. Generally, this difference was less than 1%.

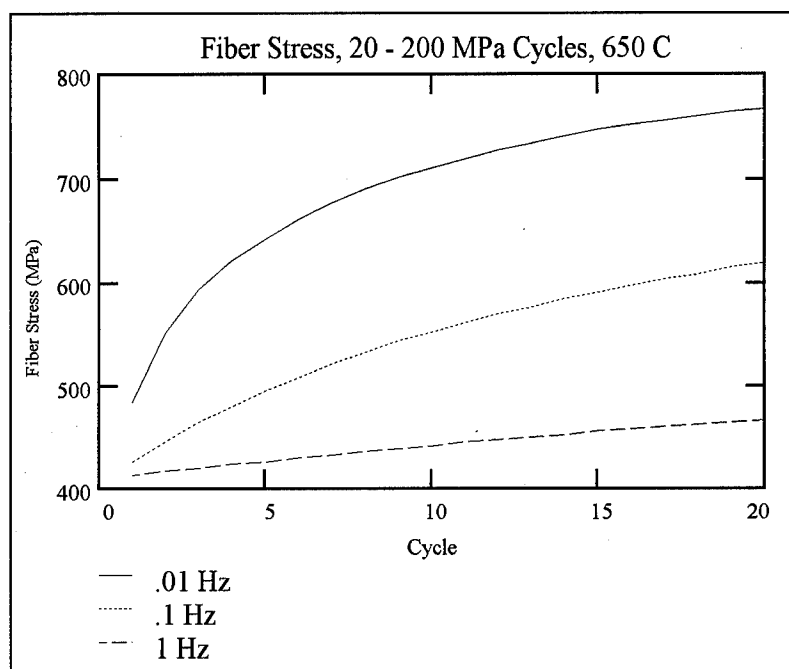


Figure 20. SCS-6/Ti- β 21s Cross Ply Fiber Microstress vs Cycle, 650°C Isothermal

The resulting microstresses were then curve fitted in MathCad for ease of use. A second order polynomial proved to perform well at approximating the microstresses as a function of the applied composite stress. Figure 21 shows the data points and the resulting curve fits for the fiber stress in a cross-ply laminate. The curve fit equations for the fiber are given in Equation (63) where σ is the maximum stress applied to the laminate. The fiber stress includes *LISOL*'s predictions for both the thermal and mechanical stresses, while the matrix stress represents the change in stress for a given cycle.

$$\sigma_f(\sigma) = \begin{cases} 5.735 \times 10^{-4} \sigma^2 + 3.740 \sigma - 212 & \text{for 1 Hz} \\ 2.589 \times 10^{-4} \sigma^2 + 4.334 \sigma - 228 & \text{for 0.1 Hz} \\ 1.480 \times 10^{-4} \sigma^2 + 5.015 \sigma - 224 & \text{for 0.01 Hz} \end{cases} \quad (63)$$

Equation (64) show the results when this process was applied for the matrix stresses.

$$\sigma_m(\sigma) = \begin{cases} -2.488 \times 10^{-4} \sigma^2 + .592 \sigma & \text{for 1 Hz} \\ -5.643 \times 10^{-5} \sigma^2 + .346 \sigma & \text{for 0.1 Hz} \\ 5.154 \times 10^{-5} \sigma^2 + .092 \sigma & \text{for 0.01 Hz} \end{cases} \quad (64)$$

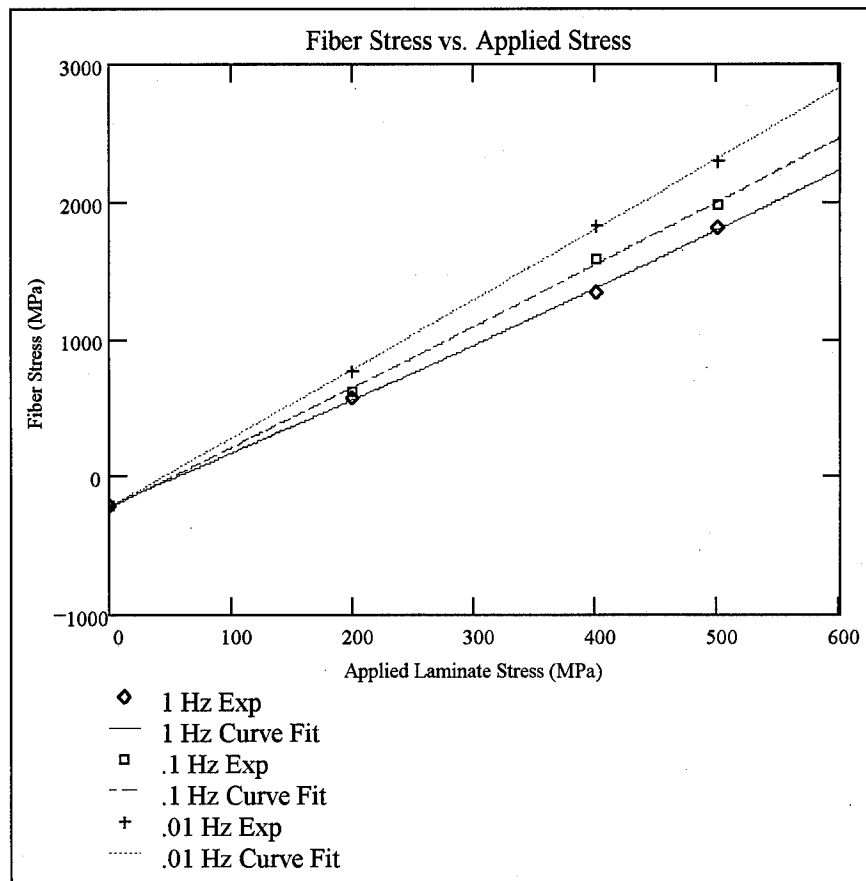


Figure 21. SCS-6/Ti-β21s Cross Ply Fiber Microstress vs Applied Stress, 650°C Isothermal

4.2.2 SCS-6/Ti- β 21s Cross Ply Isothermal Fatigue

Once microstress functions were developed, they were inserted into the equations for N_m and N_f and combined into the linear damage accumulation model. The S-N curves generated by the model for the various frequencies were then compared to experimental data. The constants were then varied to produce the best match among isothermal, in-phase thermomechanical, and out-of-phase thermomechanical fatigue. This occurred with the following values:

$$B_m = 1.4 \times 10^{18} \quad n_m = 5.5 \quad p = 0.75 \quad N_0 = 6.8 \quad \sigma_0 = 3500$$

The resulting S-N curves are shown in Figure 22.

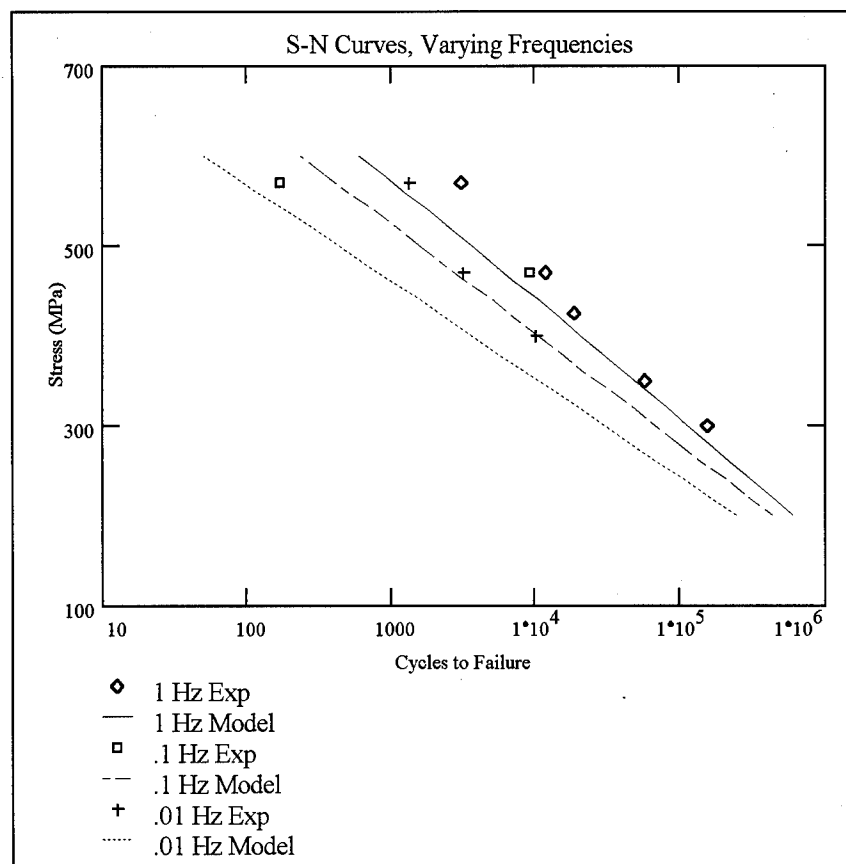


Figure 22. SCS-6/Ti- β 21s Cross Ply, 650°C Isothermal

4.2.3 SCS-6/Ti- β 21s Cross Ply Thermomechanical Fatigue

The entire process was repeated for thermomechanical fatigue for 3 minute in-phase and out-of-phase cycles from 150°C to 650°C. Once again the load ratio, R , was set to be 0.1. Figure 23 shows the fiber microstress as determined by *LISOL* over the course of the first 20 cycles.

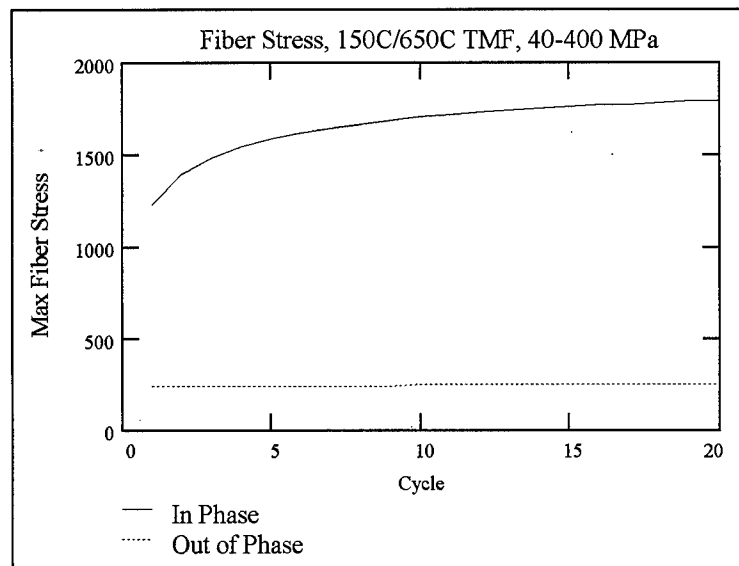


Figure 23. SCS-6/Ti- β 21s Cross Ply Fiber Stress, In-Phase & Out-Of-Phase TMF, 3 Min 150°C/650°C Cycles

As Figure 23 demonstrates, the viscoplastic effects as shown by the change in the 0° fiber stress are fairly well stabilized by the 20th cycle. The differences between the fiber stresses in the 19th and 20th cycles for in-phase and out-of-phase fatigue are 0.3% and 0.2%, respectively. The values of the microstresses were imported into MathCad, and the curve fitting was accomplished similarly to the microstress function generation for

isothermal fatigue, except that $\Delta\sigma_m$ could be fairly accurately modeled with a linear polynomial. Fiber stress, σ_f , is still modeled with a quadratic equation.

When the empirical constants listed in the previous section were inserted into the model, they produced the S-N curves for in-phase (IP) and out-of-phase (OP) thermomechanical fatigue as shown in Figure 24.

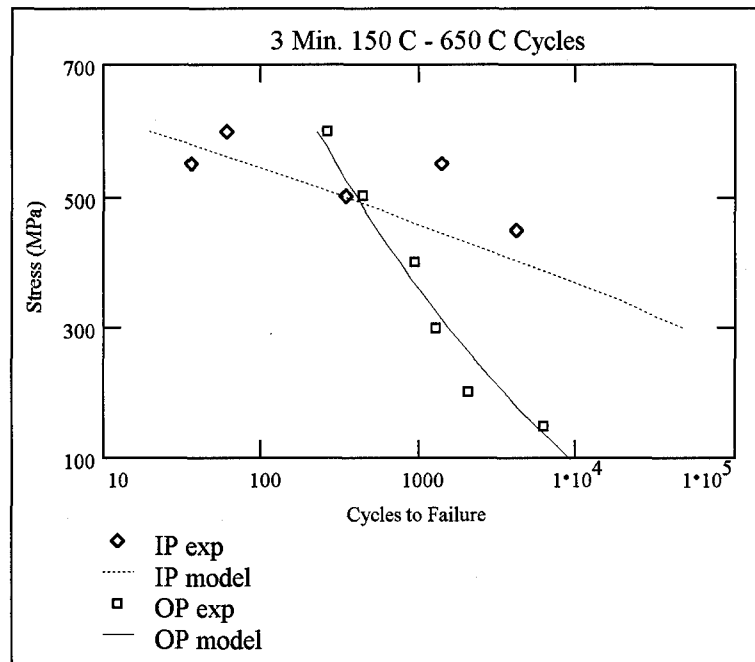


Figure 24. SCS-6/Ti-β21s Cross Ply, 150°C/650°C TMF

4.2.4 TMF Modeling of Other SCS-6/Ti-β21s Lay-ups

The present model was also applied to quasi-isotropic $[0/\pm 45/90]_s$ and unidirectional lay-ups under thermomechanical fatigue loading using the same constants as generated for Sections 4.2.2 and 4.2.3. The cycle length remained at 3 minutes, and the load ratio stayed at 0.1. In each case, as with the cross ply laminate, the fiber and matrix microstresses were taken from the 0° ply in the 20th cycle as generated by *LISOL*.

Figures 25 and 26 show the S-N curves predicted by the model along with experimental data.

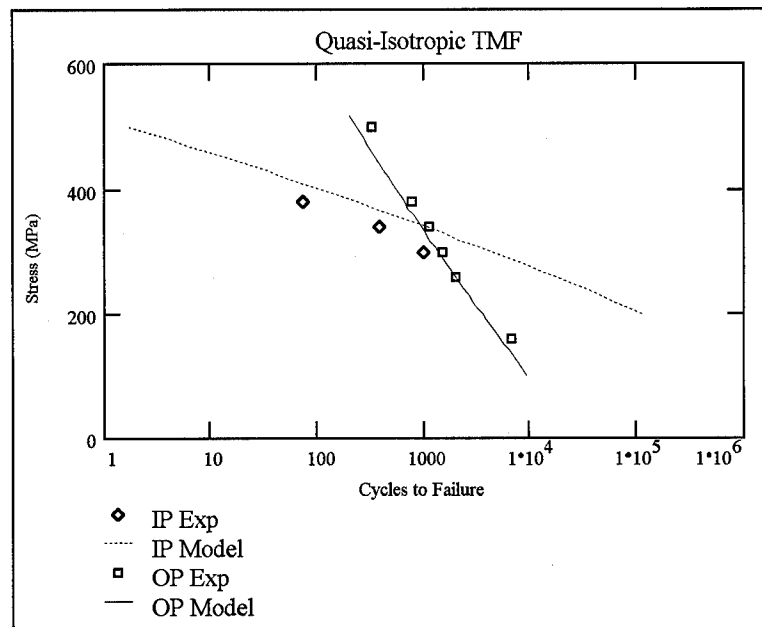


Figure 25. SCS-6/Ti- β 21s Quasi-Isotropic, 150°C/650°C TMF

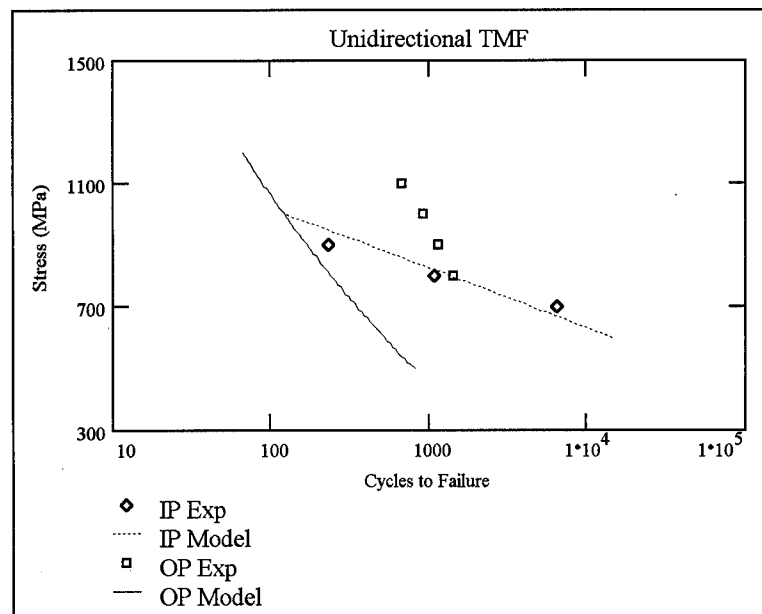


Figure 26. SCS-6/Ti- β 21s Unidirectional, 150°C/650°C TMF

The model is fairly accurate at predicting thermomechanical fatigue behavior for the quasi-isotropic laminate while using the same empirical constants as developed for cross ply laminates. Due to the presence of different failure mechanisms between unidirectional composites and those containing off axis lamina, the model underpredicts out-of-phase thermomechanical fatigue life in the unidirectional case by roughly one order of magnitude. Figure 27 shows predictions for unidirectional lay-ups with the constant n_m revised to be 5.2 instead of 5.5.

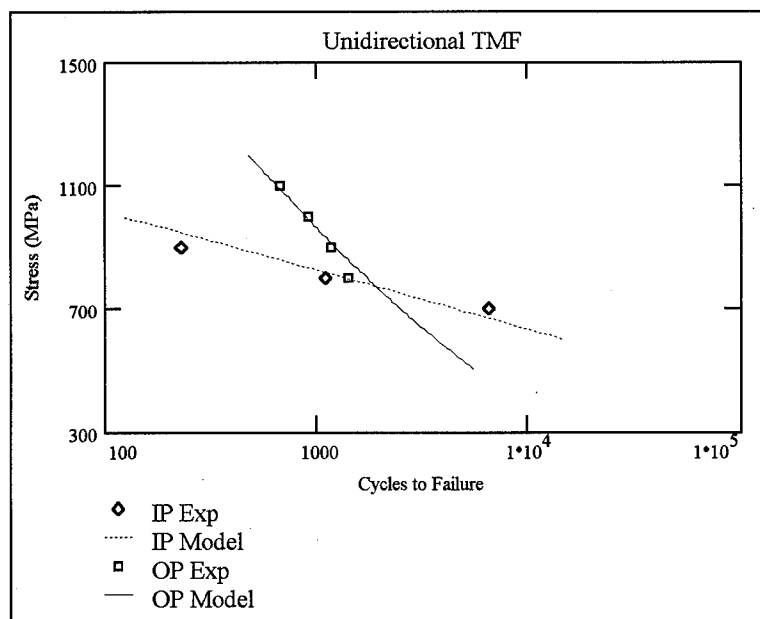


Figure 27. SCS-6/Ti-β21s Unidirectional, TMF, Revised n_m

4.2.5 SCS-6/Ti-15-3 Cross Ply Isothermal Fatigue

The model was also applied to fatigue of laminates with titanium 15-3 as the matrix. As with the SCS-6/Ti- β 21s system, the microstresses were determined by *LISOL*, and a single set of empirical constants was developed for use in both isothermal and thermomechanical fatigue. First, the cross-ply configuration was examined under isothermal fatigue at 427°C. With the Ti-15-3 matrix, the fiber stresses were nearly constant (less than 1% deviation between the 1st and 20th cycles). For consistency, the microstresses were still taken from the 20th cycle. The constants developed for the fatigue of SCS-6/Ti-15-3 are as follows:

$$B_m = 1.4 \times 10^{18} \quad n_m = 5.35 \quad \sigma_0 = 2500 \quad p = .75 \quad N_0 = 6.5$$

The resulting S-N curve for isothermal fatigue at 427°C is shown in Figure 28.

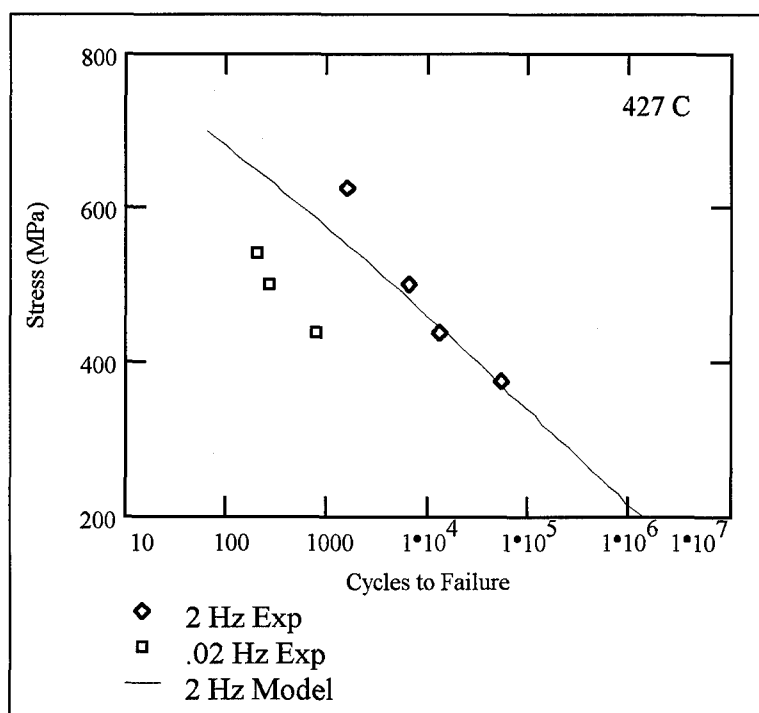


Figure 28. SCS-6/Ti-15-3 Cross Ply, 427°C Isothermal

In this case, the model did not show any difference between frequencies. As discussed in Section 4.1.4, at 427°C, load rate effects are minimal for titanium 15-3, and the micromechanics model does not account for time dependent behavior in the fiber matrix interface. Thus, the model could predict the fatigue life at the two different frequencies. Emphasis was placed on matching the higher frequency data to minimize the time dependent effects on interface degradation.

4.2.6 SCS-6/Ti-15-3 Laminate Thermomechanical Fatigue

The model was also applied to cross ply and quasi-isotropic SCS-6/Ti-15-3 laminates under thermomechanical fatigue loading. The temperature was cycled between 149°C and 427°C both in-phase and out-of-phase with the mechanical loading. The cycle period was 48 seconds, and the load ratio was 0.1. Unlike in the isothermal case, the fiber stresses do not remain constant over the first 20 cycles. Figure 29 shows this behavior.

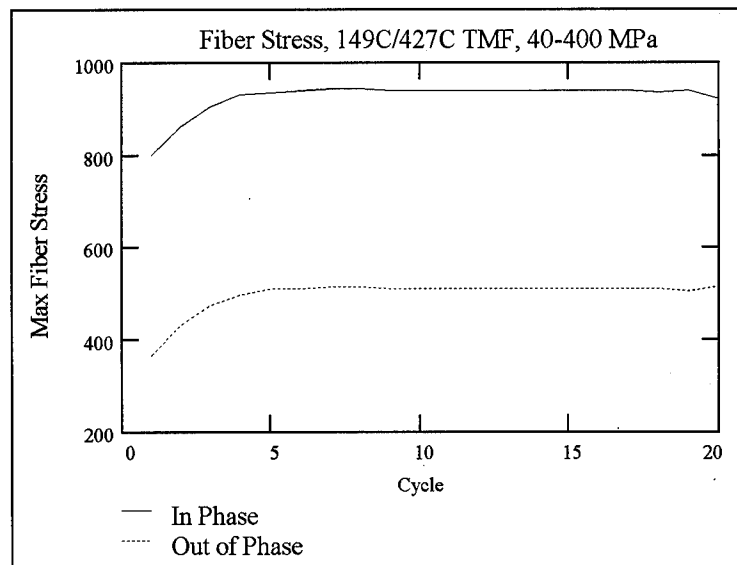


Figure 29. SCS-6/Ti-15-3 Cross-Ply Fiber Stresses, 149°C/427°C TMF

As can be seen in Figure 29, the fiber stress actually plateaus at about the 4th or 5th cycle.

The microstresses used in the fatigue model were the values at these plateaus.

Figures 30 and 31 show the resulting S-N curves for in-phase (IP) and out-of-phase (OP) thermomechanical fatigue for the two laminates when the constants in Section 4.2.5 are used.

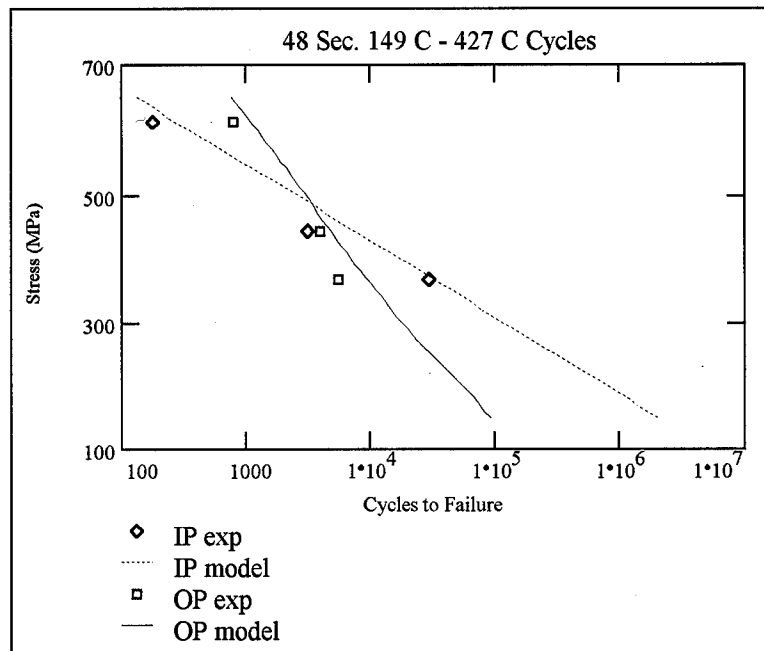


Figure 30. SCS-6/Ti-15-3 Cross Ply, 149°C/427°C TMF

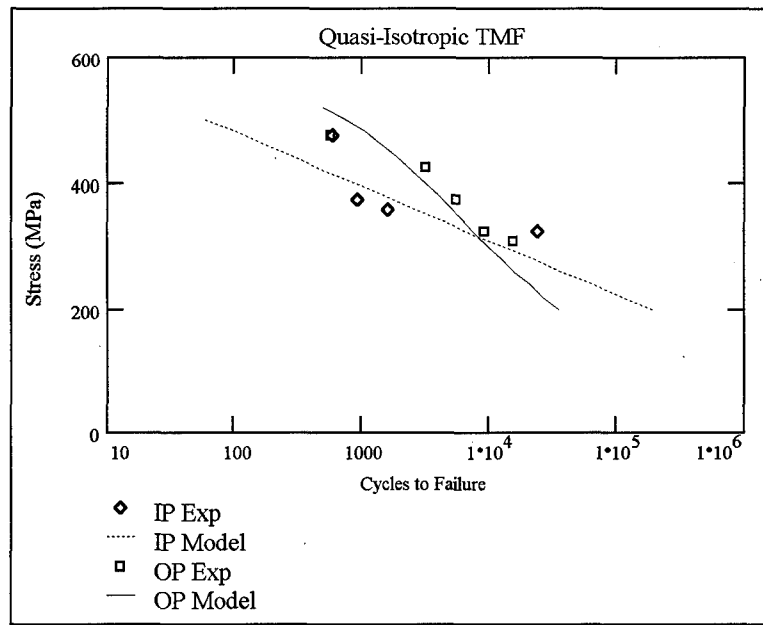


Figure 31. SCS-6/Ti-15-3 Quasi-Isotropic, 149°C/427°C TMF

4.2.7 Linear Damage Accumulation Model Discussion

Using micromechanics to account for the time-dependent behavior of a composite under fatigue in a linear damage accumulation model was found to correlate well with experimental data for a variety of load cases and laminates. A wide range of frequencies were examined using this method for cross ply SCS-6/Ti-β21s under isothermal fatigue loading. The temperature, 650°C, was high enough such that a difference in load rate produced a dramatic difference in stress strain behavior (see section 4.1). A comparison of predicted cycles to failure and the actual cycles to failure is shown in Figure 32. It can be seen in this figure that the model does the best at predicting the composite's behavior in the mid-range of cycles to failure. For both high-cycle and low-cycle fatigue, the predicted results tend to deviate from the actual results, although only by less than one order of magnitude. The deviation for high cycle fatigue can be accounted for in large

part by limitations in the original model. As σ , and therefore, σ_f and $\Delta\sigma_m$, approaches 0, N_m approaches ∞ as expected, but N_f approaches 10^{N_0} . Thus the cycles to failure of the composite approaches a finite number as the fatigue load approaches 0. This occurs at all frequencies and temperatures.

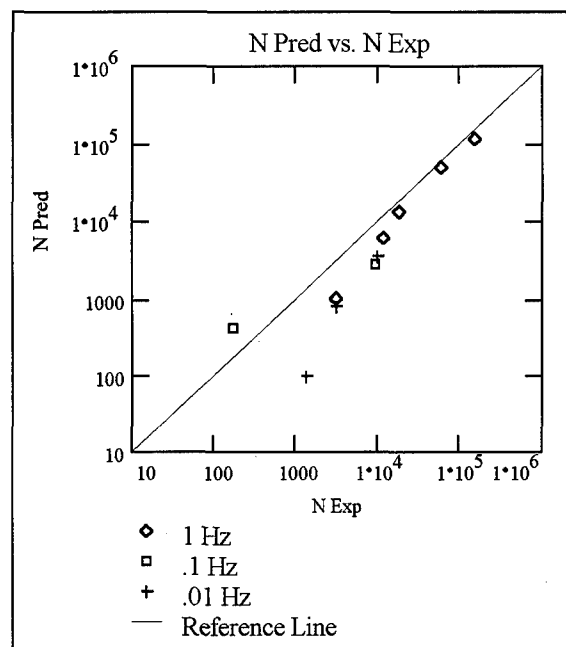


Figure 32. SCS-6/Ti- β 21s Cross Ply, 650°C Isothermal, N_{pred} vs. N_{exp}

At 427°C, the model was unable to accurately predict the effects of changing frequencies for isothermal fatigue of SCS-6/Ti-15-3 cross ply laminates. This is due to the fact that the micromechanics model only uses the viscoplastic behavior of the matrix material to evaluate time dependent phenomena. As discussed in section 4.1, at 427°C and below, titanium 15-3 is only minimally affected by the rate of load. Thus, the micromechanics model returns nearly identical values for the microstresses even at different frequencies. The degradation of the interface is most probably dependent upon

load rate, but this is totally unaccounted for by the micromechanics model. This results in underprediction of the load rate effects at the higher temperatures and load rate independent predictions at the lower temperatures.

To limit the time dependent effects, emphasis was placed on predicting the behavior for high frequency fatigue. This resulted in good correlation to the experimental data for isothermal fatigue at 427°C and 2 Hz. Figure 33 compares the actual and predicted fatigue life for this load case.

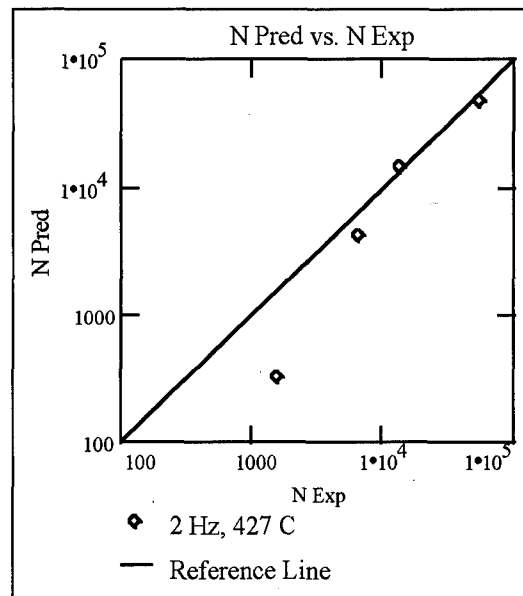


Figure 33. SCS-6/Ti-15-3 Cross Ply, Isothermal N_{pred} vs N_{exp}

Both the fiber and matrix microstresses used in this model were measured in the 0° ply. The fiber stresses in the 90° lamina were a small fraction of those in the 0° ply. The matrix stresses in the off axis ply were lower than in the on-axis layer by only about 15% in the worst case. The microstresses were also measured during the 20th cycle to allow the viscoplastic effects to stabilize. By the 20th cycle, either a plateau value of fiber stress

was reached, or the difference in the fiber stress between consecutive cycles was less than 1%. This behavior was seen for both isothermal and thermomechanical fatigue. The matrix microstresses behaved in a similar manner, except that while the fiber stress increased over cycles, the matrix stress decreased.

The present model correlated well with the behavior of cross ply laminates under thermomechanical fatigue loading. Figure 34 compares the predicted cycles to failure to the actual cycles to failure for both in-phase and out-of-phase fatigue. The temperature range of the cycle was 150°C to 650°C. The accuracy of the model is significantly greater for out-of-phase thermomechanical fatigue than for in-phase. This is probably due to the greater scatter in the in-phase fatigue data at this temperature and for this laminate. Other load cases and laminates show better correlation for both types of thermomechanical

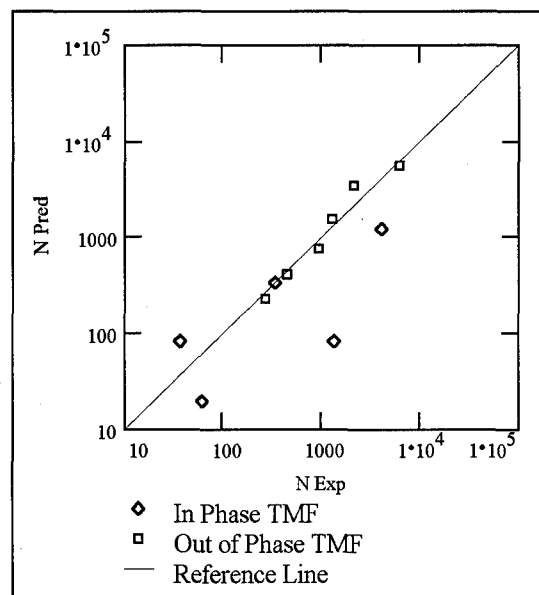


Figure 34. SCS-6/Ti-β21s Cross Ply, TMF N_{pred} vs N_{exp}

fatigue. This is shown to be true for SCS-6/Ti-15-3 cross ply laminates in Figure 35 where the predicted fatigue life is very close to the experimental fatigue life for both in-phase and out-of-phase thermomechanical fatigue.

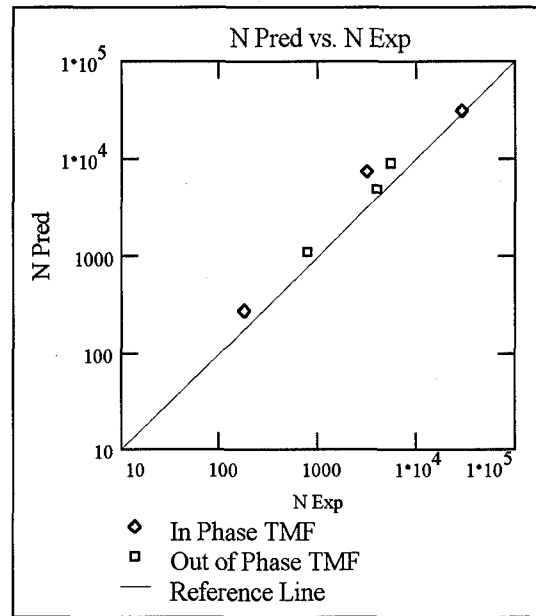


Figure 35. SCS-6/Ti-15-3 Cross Ply, TMF N_{pred} vs N_{exp}

Even with similar model limitations as in the isothermal fatigue case, the model provides a good estimate of thermomechanical fatigue life of both SCS-6/Ti- β 21s and SCS-6/Ti-15-3 cross ply composites. The out-of-phase data are matched within a quarter order of magnitude, and, even in the worst case, the in-phase data are matched within one order of magnitude.

The results when the present model was applied to quasi-isotropic lay-ups in thermomechanical fatigue were quite good while using the same constants as for cross-ply isothermal and thermomechanical fatigue. Figures 36 and 37 compare the predicted fatigue life with actual fatigue life for quasi-isotropic laminates with titanium β 21s and

titanium 15-3 matrices, respectively. The model had a tendency to overpredict the in-phase thermomechanical fatigue life of the SCS-6/Ti-b21s by roughly a half order of magnitude.

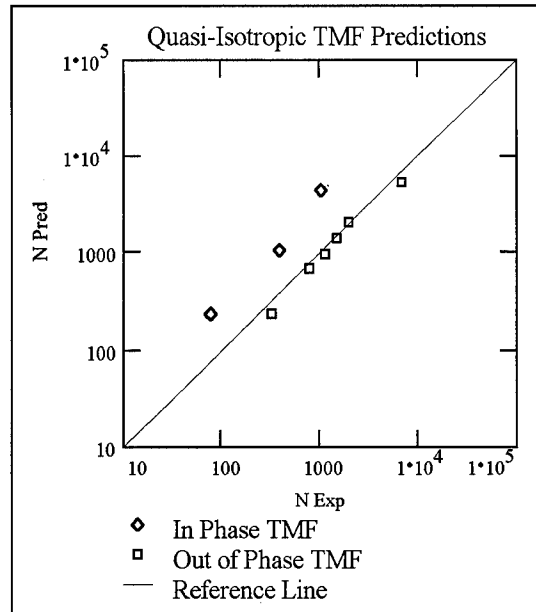


Figure 36. SCS-6/Ti- β 21s Quasi-Isotropic, TMF N_{pred} vs N_{exp}

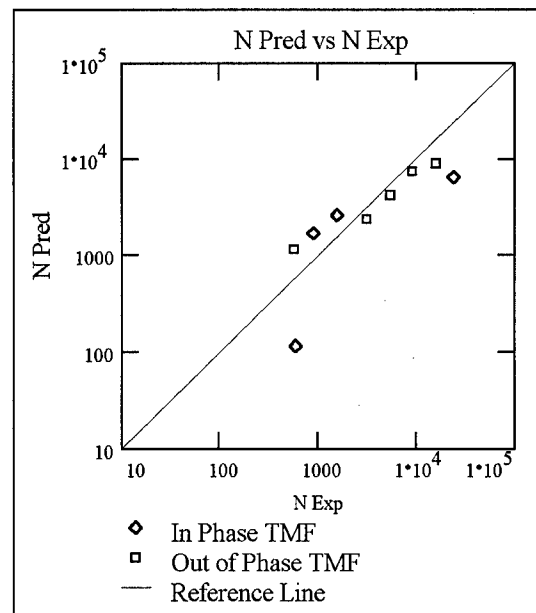


Figure 37. SCS-6/Ti-15-3 Quasi-Isotropic, TMF N_{pred} vs N_{exp}

Because there was more scatter in the data for SCS-6/Ti-15-3, the model's correlation was not as good as that for SCS-6/ β 21s. The microstresses for this lay-up were also taken from the 0° ply. Once again, the fiber stress in the axial ply was much greater than the fiber stress in any of the off-axis plies. The matrix stress in the 0° layer was within 20% of the matrix stress in the other plies, and thus, could be used as the representative microstress for the matrix material.

Application of the model to unidirectional composites under thermomechanical fatigue loading initially produced less accurate results. The model tended to underpredict the out-of-phase fatigue life by almost an order of magnitude for every load point due to different failure mechanisms. Unlike in cross ply and quasi-isotropic layups, the fiber matrix interface is not subjected to normal stresses in a unidirectional composite under axial load. Minor adjustments to the empirical constants yielded much better results as shown in Figure 27 in Section 4.2.4, but clearly does not satisfy the original goal of establishing a single set of constants for each layup composition and maximum temperature. The fatigue life predicted by the original constants is compared to the experimental fatigue life in each case in Figure 38.

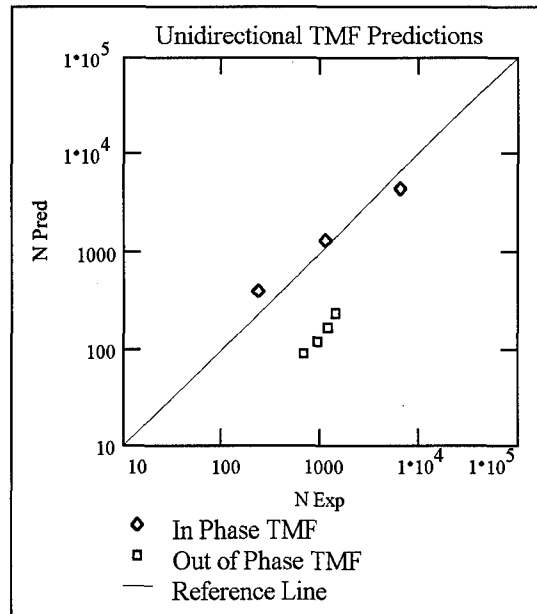


Figure 38. SCS-6/Ti-β21s Unidirectional, TMF N_{pred} vs N_{exp}

A single set of constants can be used to correlate within a single order of magnitude with isothermal and both in-phase and out-of-phase thermomechanical fatigue data for each material. Because the micromechanics model does not address time dependent behavior in the fiber matrix interface, the predicted behavior is independent of frequency at temperatures less than 450°C. The matrix microstresses tend to be much greater for out-of-phase fatigue than for in-phase by about a factor of 3 at high stresses. Conversely, the fiber stress is higher in in-phase fatigue. Altering the constants in N_m (B_m and n_m) tends to shift the out-of-phase curve, while changing the constants in N_f (N_0 , σ_0 , and p) tends to shift the in-phase curve. Each of these curve shifts leaves the other curve relatively unaffected.

The model could probably be enhanced by readdressing the form of N_f . Currently, as σ_f approaches 0, N_f approaches some finite number. Ideally, N_f should approach infinity as σ_f approaches 0. Even with this potentially major flaw, the present model is able to provide at least, and usually better than, a rough order of magnitude estimate on the fatigue life of cross ply, quasi-isotropic, and unidirectional composites.

4.3 Constituent Based Fatigue Model

The objective of the final phase of the present effort was to develop a fatigue model for cross ply laminates based on the behavior of the constituent materials under fatigue loading. The model is based on linear damage accumulation similarly to the model described in section 4.2. The axial direction fatigue is assumed to behave as follows:

$$\frac{1}{N_{0\text{-ply}}} = \frac{1}{N_f} + \frac{1}{N_m} \quad (65)$$

where N_m is the fatigue life of the homogeneous matrix material, and N_f is the fatigue life of the fiber material. Both of these are based on the microstresses determined by the micromechanics model, *LISOL*. The fatigue life of the 90° ply is assumed to be:

$$\frac{1}{N_{90\text{-ply}}} = \frac{1}{N_f} + \frac{1}{N_m} + \frac{1}{N_I} \quad (66)$$

where N_I represents the effect on fatigue life due to interface damage. Once again, all inputs were microstresses and interface damage determined by *LISOL*.

Once fatigue life for the individual layers were determined, the single ply information was combined to produce a fatigue life prediction for the entire cross ply composite. Several methods were examined to accomplish this including linear damage

accumulation and geometric averaging. In all cases, the predictions by the model were compared to preexisting experimental data [37-39]. The subject material for this phase was SCS-6/Ti-15-3. The Bodner-Partom constants developed in Section 4.1 were used for all the micromechanics calculations.

4.3.1 Matrix Fatigue Behavior

The matrix material was assumed to behave similarly to the model developed by Nicholas, et al. [5-8] as in the following equation:

$$N_m = B_m (\Delta\sigma_m)^{-n_m} \quad (67)$$

The constants B_m and n_m were determined to be 2×10^{17} and 5, respectively, by comparing the S-N curve predicted by Equation (67) and experimental data [38] for titanium 15-3 under isothermal fatigue loading. Figure 39 shows the comparison.

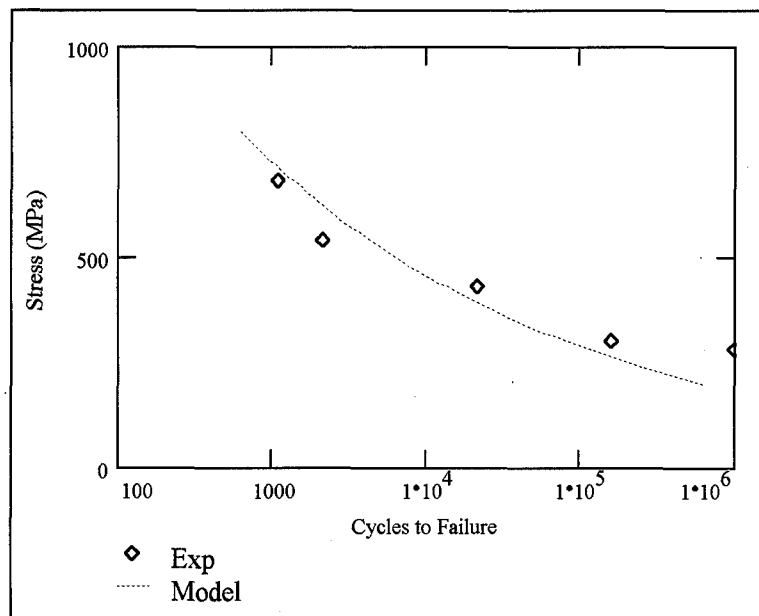


Figure 39. Ti-15-3, Isothermal Fatigue S-N, 25°C

4.3.2 Fiber and 0° Ply Fatigue Behavior

As with the matrix material, the fiber material was assumed to behave as in section 4.2 with slight modification:

$$N_f = 10^{N_0 \left(1 - \frac{\sigma_f}{\sigma_{ult}}\right)} \quad (68)$$

In this equation, σ_{ult} is the ultimate strength of the fiber, 4400 MPa. When σ_f is equal to σ_{ult} , N_f equals 1, and the fiber breaks on the first cycle. Another result is that there is only one empirical constant to determine. Unlike the function for N_f in the previous section, there is no load ratio factor.

Since there was no fatigue data for the fiber material available for this study, it was necessary to derive the fiber fatigue behavior from the behavior of the matrix material and 0° laminates. This was done by using the function for N_m determined in section 4.3.1 and varying the fiber constants until a good match was achieved between the N_{0-Ply} developed by the model and previously developed experimental data for a unidirectional laminate under axial fatigue [38]. The stresses used in the model were the microstresses as determined by *LISOL*. For the unidirectional case, the fiber and matrix microstresses behave in a nearly linear fashion. The equations, $\sigma_m = 0.49 \sigma$ and $\sigma_f = 1.977 \sigma - 716$, were used to provide continuous functions of the fiber and matrix stresses, respectively. After several iterations, the optimum model performance was accomplished when N_0 was equal to 7.5. This predicts that the fiber material is significantly stronger in fatigue than the matrix material which is expected. Figures 40 and 41 show the fiber and unidirectional fatigue behaviors, respectively.

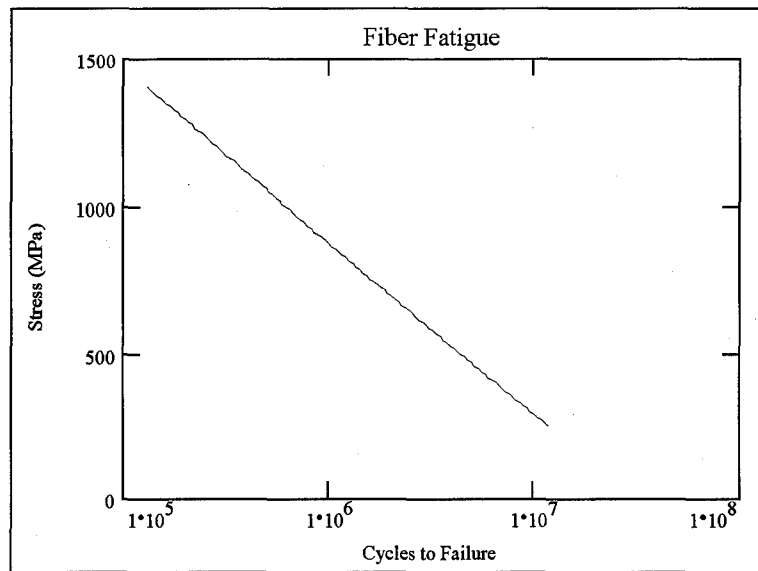


Figure 40. SCS-6, Isothermal Fatigue Model, 25°C

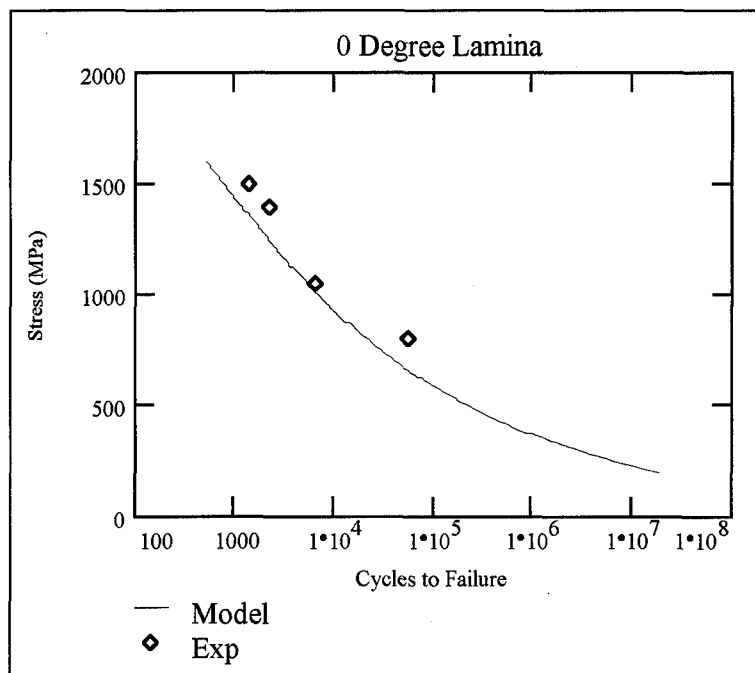


Figure 41. SCS-6/Ti-15-3 0° Ply, Isothermal Fatigue, 25°C

4.3.3 Interface and 90° Ply Fatigue Behavior

Since functions for N_m and N_f were determined previously in sections 4.3.1 and 4.3.2, respectively, only the interface damage term, N_I , needs to be defined to predict the fatigue life of a 90° ply. The process for determining N_I has three stages. The first step is to determine from *LISOL* at what cycle the interface has completely failed for several different applied stresses. When the interface has failed, the microstresses in the fiber go to 0. In effect, this produces an S-N curve for the interface between the fiber and the matrix. Once the “S-N” data points are developed, they are then fit with a function. This function is then shifted so that it matches the experimental data when combined with the fiber and matrix fatigue terms.

The function describing the interface fatigue life as developed by step one of the above procedure is as follows:

$$N_I = 10^{(5.456 - 5.23 \times 10^{-8} \sigma^3 + 95.181 \sigma^{-1})} \quad (69)$$

where σ is the stress seen by the 90° ply. This function was then modified to fit the 90° fatigue data:

$$N_I = 10^{(3 - 5 \times 10^{-8} \sigma^3 + 95 \sigma^{-1})} \quad (70)$$

The two above functions are plotted in Figure 42. The shift in the curve described by Equation (69) to that described by Equation (70) can be accounted for by the fact that a crack in the interface tends to extend beyond the interface itself and into the matrix material creating a further weakness in the composite. Also, crack propagation along the interface due to fatigue crack growth is not accounted for in the micromechanics model. A realistic fatigue life model must include this effect.

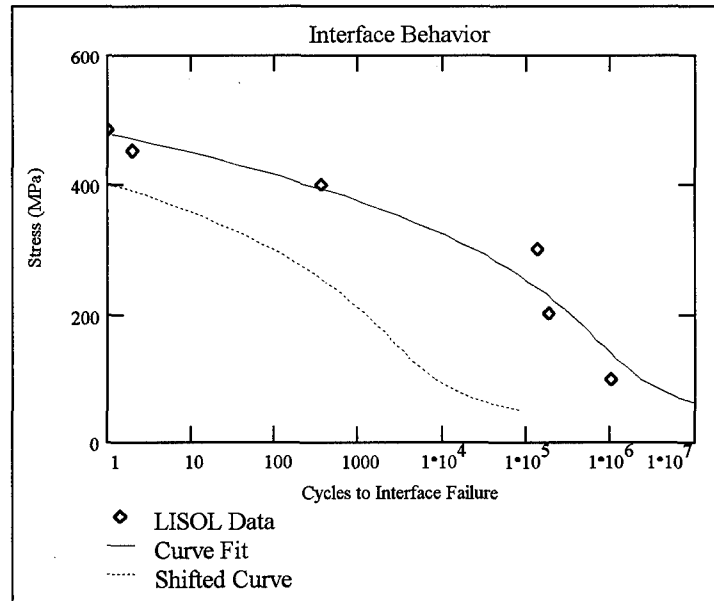


Figure 42. SCS-6/Ti-15-3 90° Ply, Interface Damage, Iso. Fatigue, 25°C

The resulting model predictions for isothermal fatigue of a 90° ply at room temperature are shown in Figure 43 along with experimental data [38].

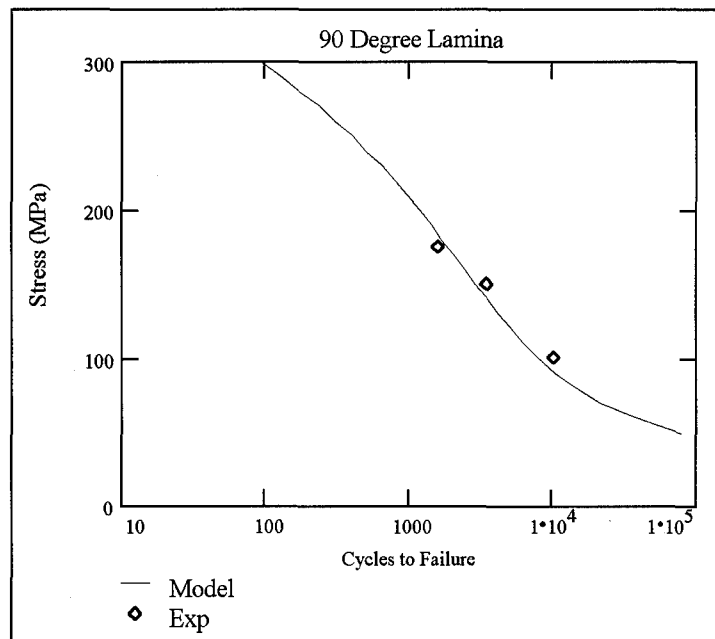


Figure 43. SCS-6/Ti-15-3 90° Ply, Isothermal Fatigue S-N, 25°C

4.3.4 Cross Ply Fatigue Behavior

Once the life prediction models were established for the 0° and 90° plies, they were then combined to predict cross ply laminate behavior under isothermal fatigue at room temperature. The layer stresses were determined using *LISOL* and then curve fitted using mathcad. For isothermal fatigue at room temperature, the lamina stresses remain nearly constant (less than 1% deviation between the 1st and 20th cycles). The 0° ply stress as a function of applied stress is given as

$$\sigma_{0\text{-ply}} = 1.456\sigma_{x\text{-ply}} + 2.475 \times 10^{-4}\sigma_{x\text{-ply}} - 130 \quad (71)$$

and the stress in the 90° ply is given as

$$\sigma_{90\text{-ply}} = 0.544\sigma_{x\text{-ply}} - 2.475 \times 10^{-4}\sigma_{x\text{-ply}} + 130 \quad (72)$$

These two function are plotted against the applied laminate stress in Figure 44.

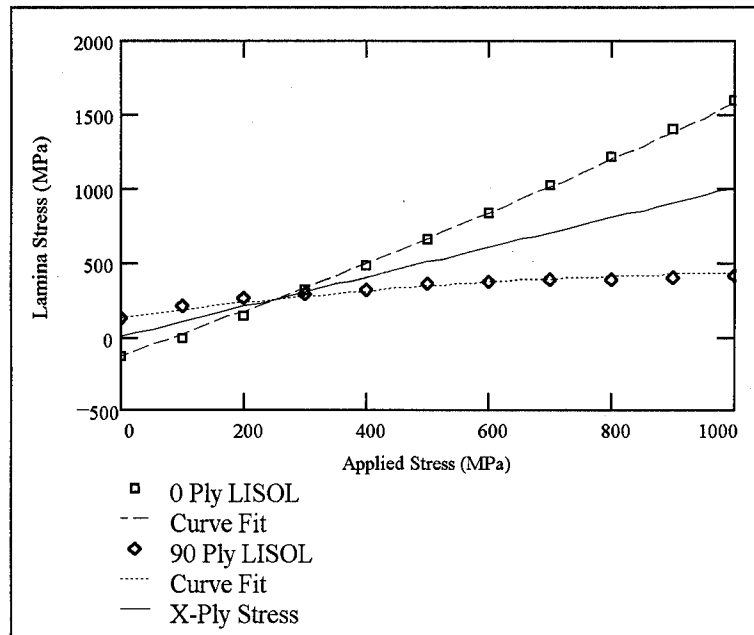


Figure 44. SCS-6/Ti-15-3 Cross Ply Lamina Stresses

Throughout the stress range, the 0° ply carries a large majority of the stress.

Several methods of combining the 90° and 0° models to predict cross ply laminate fatigue behavior were considered, including linear damage accumulation and various forms of averaging. However, simply using the microstresses of the 0° ply seemed to produce a good estimation of the fatigue behavior of the cross-ply composite. Figure 45 shows the fatigue life predictions of the 0° and 90° layers with the microstresses seen in a cross-ply laminate applied. The figure also contains the applicable experimental data for comparison.

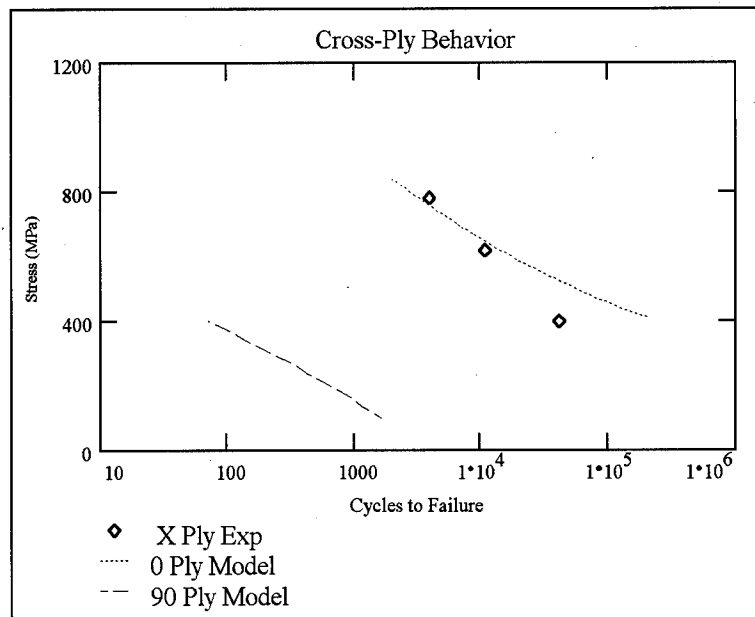


Figure 45. SCS-6/Ti-15-3 Cross Ply, Isothermal Fatigue, 25°C, Individual Lamina Predictions

4.3.5 Constituent Fatigue Model Discussion

The constituent fatigue model (Sections 4.3.1 - 4.3.4) was reasonably accurate in predicting the behavior of 0° , 90° , and cross ply laminates under isothermal fatigue

loading at room temperature. Room temperature was chosen to minimize the effects of strain rate. At this temperature, the microstresses remained almost constant (less than 1% change over 20 cycles) during the cyclic loading. As a result, the microstresses from the 1st cycle yield results equal to the those produced by the 20th cycle microstresses. The only stress-controlled fatigue data for homogeneous titanium 15-3 had a load ratio of 0.1 or 0 [38, 39].

The assumed form of N_f is the same as that used in Section 4.2 and developed in previous literature [5]. As a result, the same limitations exist in this model. When σ_f approaches 0, N_f should approach infinity, but instead, it approaches a finite number, 10^{N_0} . Because the *in situ* fatigue behavior of the SCS-6 fibers is difficult to determine, the necessary constants for N_f were determined by matching 0° ply fatigue data.

The fiber-matrix interface fatigue term, N_i , was developed through a combination of *LISOL* and empirical comparison to experimental data for 90° laminate fatigue. The result was a curve that predicted a greater level of damage than the results from *LISOL*. This could be used to account for any cracks in the matrix material that extend beyond the area of the fiber-matrix interface and for fatigue crack growth along the interface. The prediction for the fatigue life of the 90° plies turned out to be quite accurate using this method.

A simple but effective approach in predicting the fatigue behavior of the cross ply laminate is to assume the 0° ply dominates the behavior. Therefore, the composite fatigue life is equal to the fatigue life of the 0° ply calculated using the microstresses determined by *LISOL*. This method was more accurate than any of the other combination techniques

considered. Using the 0° ply microstresses was also the basis of the model described in section 4.2. The accuracy in this application helps validate the use of the 0° layer microstresses to predict the behavior of a composite with a combination of 0° and off-axis plies as proposed in previous literature [32].

4.4 Consolidated Constants Tables

This section provides summary tables of all of the constants developed by the present effort. The original presentation of each set of constants can also be found in Sections 4.1, 4.2, and 4.3.

4.4.1 Bodner Partom Viscoplastic Constants (Ti-15-3)

Table 4. Temp. Dependent Bodner-Partom Constants

Temp (°C)	E (GPa)	Z ₂ (MPa)	Z ₃ (MPa)	n	a ₁ = a ₂ (sec ⁻¹)	m ₂ (MPa ⁻¹)
25	86.3	1200	250	4.5	10 ⁻⁸	.005
315	80.4	1070	454	2.9	4.4x10 ⁻⁶	.04
427	77.5	1020	550	2.7	10 ⁻⁵	.05
482	72.2	850	1100	1.6	1	5
566	64.4	750	2400	1.05	2.5	15
650	53.0	650	3000	0.9	3	20

Temperature independent constants:

$$D_0 = 10^4 \text{ s}^{-1} \quad Z_1 = 1300 \text{ MPa} \quad r_1 = 3 \quad r_2 = 3 \quad m_1 = 0 \text{ Mpa}^{-1}$$

4.4.2 Linear Damage Accumulation Model Constants

Table 5. Linear Damage Accumulation Model Constants

Load Case	B_m	n_m	N_0	σ_0	p
SCS-6/Ti- β 21s Max Temp 650°C	1.4×10^{18}	5.5*	6.8	3500	0.75
SCS-6/Ti-15-3 Max Temp 427°C	1.4×10^{18}	5.35	6.5	2500	0.75

* For a more exact fit of a unidirectional laminate under 150°C/650°C thermomechanical fatigue, n_m can be set to 5.2 at a cost of a loss of accuracy for all of the other tested laminates ([0/90], [0/±45/90]).

4.4.3 Constituent Based Model Constants

Table 6. Constituent Based Model Constants

Load Case	B_m	n_m	N_0	σ_0	p
[0/90] Iso, 25°C SCS-6/Ti-15-3	2×10^{17}	5	7.5	4400	0

Since the constants for the cross ply case were developed from the behavior of the 0° and 90° orientations, the constants in Table 6 can also be used to predict the behavior of unidirectional SCS-6/Ti-15-3 under axial or transverse isothermal fatigue loading.

V. Conclusions And Recommendations

Because of their high strength, light weight, and resistance to high temperatures, titanium based metal matrix composites have received a lot of attention in recent years for aerospace applications. Unlike polymeric matrix composites, the matrix material in a metal matrix composite contributes significantly to the overall mechanical properties of the composite. It is therefore necessary to understand the micromechanical behavior of the laminate to be able to model its macroscopic behavior. Since the plastic effects of titanium are time dependent, a viscoplastic theory must be used to accurately predict the reactions of the titanium matrix material in the micromechanics model.

The high cost of titanium based metal matrix composites makes an accurate fatigue behavior model highly desirable. There have been several fatigue models developed in the past [5-8, 28-33], but few that use the composite microstresses to account for the micromechanic behavior [5-8, 31]. Of these, none uses a unified viscoplastic theory with the capability to model interface damage, and nearly all are purely empirical. The goals of the present effort are to fully characterize the viscoplastic behavior of titanium 15-3 using the Bodner Partom unified theory with directional hardening [1, 2, 16], incorporate time dependent micromechanics in a previously developed linear damage accumulation model [5-8], and develop a new model based at least partially on the constituent properties.

5.1 Conclusions

(1) Titanium 15-3 was characterized using the Bodner Partom unified viscoplastic theory with directional hardening. Constant strain rate tests were accomplished on titanium 15-3 at 25°C, 315°C, and 427°C and combined with previously performed [3]

tests at 482°C, 538°C, and 649°C to establish a complete set of data. With the use of this data, the new material parameters modeled stress strain behavior of titanium 15-3 very well. The micromechanics model with the new constants showed a marked improvement in accuracy over the previously used constants. The Bodner-Partom constants for titanium 15-3 are shown in Table 3 in Section 4.1.2 and reiterated in Section 4.4.1.

(2) Viscoplastic micromechanics information was in part successfully used to replace the time-dependent terms in a previously developed linear damage accumulation model [5-8]. The revised model produced accurate predictions for isothermal fatigue at 650°C in a cross ply SCS-6/Ti- β 21s laminate and at 427°C in a cross ply SCS-6/Ti-15-3 laminate. It also correlated well with experimental thermomechanical fatigue data for cross ply, quasi-isotropic and unidirectional layups using either matrix material. The model was able to produce these results with no changes in the constants despite changes in the layup and temperature. There were minor differences between the constants for the SCS-6/Ti- β 21s system and those for the SCS-6/Ti-15-3 system. Micromechanics information could not account for time dependent fatigue behavior when the matrix material did not exhibit viscoplastic deformation. Once the fiber matrix interface degradation algorithm is modified in the micromechanics model, it would, hopefully, be able to handle time dependent fatigue effects. The constants are summarized in Table 5 in Section 4.4.2.

(3) A new fatigue model was developed based on the fatigue behavior of the constituent properties. First, the matrix material, titanium 15-3, was modeled for isothermal fatigue [38] at room temperature using the same form as developed for the

linear damage accumulation model. This information was combined with previously developed 0° orientation fatigue data [38] to develop the fatigue behavior of the fibers. Once again, the format developed for the linear damage accumulation model was used [5]. Finally, the micromechanics model, *LISOL* [4], was used to develop a fatigue model for the fiber matrix interface. Experimental data for 90° plies [38] was used to refine the behavior estimate of the model. The model performed very well for both 0° and 90° SCS-6/Ti-15-3 laminates subjected to isothermal fatigue at room temperature.

(4) In all cases in the present study, microstresses in the 0° lamina could be used to accurately predict the fatigue life of any laminate containing 0° plies. This affirms the hypothesis that the fatigue life in such composites is governed by the behavior of the 0° layers [32]. As a composite with 0° and off-axis plies is loaded, the micromechanics can calculate what level of stress is seen by each ply. The fatigue life of the 0° ply under this stress level produces a very accurate prediction of the cross ply fatigue life when used in the constituent based model. Similar results occur when the 0° microstress calculations are used in the linear damage accumulation model.

5.2 Recommendations for Future Research

There are many areas to research in order to produce more accurate results in fatigue modeling of titanium based composites. The viscoplastic constants developed in the present effort are empirical in nature. Other researchers [18] have developed a systematic approach to determine these parameters, but it requires more data than is available at the present time. Additional constant strain rate tests should be accomplished on titanium to provide more data to develop the viscoplastic constants. This is especially

true at the higher temperatures. Additionally, some of the simplifying solutions, such as eliminating isotropic hardening and setting several of the constants equal to one another, should be reexamined.

Fatigue data, in general, are in short supply. There are very rarely more than three data points from which to try to develop a trend. This is true for nearly all lay-ups and all temperatures. Some of the data is contradictory in that identical load cases can result in dramatically different outcomes. Also, many of the fatigue tests do not result in failure. All of this results in greater difficulty in model development. Much more experimental data should be developed.

The micromechanics model, *LISOL*, should be modified to account for failure of the fibers and matrix as loading occurs. Currently, *LISOL* can account for the degradation of the fiber-matrix interface. Similar algorithms based on statistics should be developed to account for degradation in the rest of the composite. Additionally, *LISOL* needs to have the capability to address the time dependent degradation of the interface region.

The present model should be altered such that the fiber fatigue life term is based on a statistical distribution. Presently, it is linear on a semilog plot. This results in a situation where the composite will fail in a finite number of cycles even if no stress is applied. The constituent based fatigue model should also be expanded to other temperatures and to thermomechanical fatigue.

VI. References

1. Bodner, S. R. & Partom, Y., "Constitutive Equations for Elastic Viscoplastic Strain Hardening Materials." ASME Journal of Applied Mechanics, **42** (1975) 385-9.
2. Stouffer, D. C. & Bodner, S. R., "A Constitutive Model for the Deformation Induced Anisotropic Plastic Flow of Metals." International Journal of Engineering Science, **17** (1979) 757-64.
3. Rogacki, J. R. & Tuttle, M. E., "An Investigation of the Thermoviscoplastic Behavior of a Metal Matrix Composite at Elevated Temperatures." NASA Contractor Report 189706, NASA Langley Research Center, Hampton, VA (1992).
4. Robertson, D. D. & Mall S., "Micromechanical Analysis for Thermoviscoplastic Behavior of Unidirectional Fibrous Composites." Composites Science and Technology, **50** (1994) 483-96.
5. Nicholas, T., Russ, S. M., Neu, R. W., & Schehl, N., "Life Predictions of a [0/90] Metal Matrix Composite Under Isothermal and Thermomechanical Fatigue." Paper presented at the Symposium on Life Prediction Methodology for Titanium Matrix Composites, sponsored by ASTM, Hilton Head, SC, USA, 22-24 March 1994.
6. Neu, R. W., "A Mechanistic-based Thermomechanical Fatigue Life Prediction Model for Metal Matrix Composites." Fatigue & Fracture of Engineering Materials & Structures, submitted for publication, 1992.
7. Nicholas, T. & Russ, S. M., "Fatigue Life Modeling in Titanium Matrix Composites." Paper presented at the 9th Technical Conference of Composite Materials, sponsored by ASC, University of Delaware, 20-22 September 1994.
8. Russ, S. M., Nicholas, T., Bates, M. & Mall, S., "Thermomechanical Fatigue of SCS-6/Ti-24Al-11Nb Metal Matrix Composite." Failure Mechanisms in High Temperature Composite Materials, ASME, AD-Vol. **22**/AMD-Vol. **122** (1991) 37-43.
9. Findley, W. N., Lai, J. S., & Onaran, K., Creep and Relaxation of Nonlinear Viscoelastic Materials. New York: Dover Publications, Inc., 1976.
10. Torvik, P. J. & Bagley, D. L., "Fractional Derivatives in the Description of Damping Materials and Phenomena." Role of Damping in Vibrations, ASME, ed. Rogers, DE Vol. **5** (1987) 125-30.
11. Jones, D. I. G., "Viscoelastic Materials for Damping Applications." Damping Applications for Vibration Control, ASME, ed. P. J. Torvik, AMD **32** (1980) 27-51.

12. Miller, A., "An Inelastic Constitutive Model for Monotonic, Cyclic, and Creep Deformation: Part I - Equations Development and Analytic Procedures." Journal of Engineering Materials and Technology, ASME (April 1976) 97-105.
13. Walker, K. P., "Research and Development Program for Nonlinear Structural Modeling with Advanced Time-Temperature Dependent Constitutive Relationships." NASA Technical Report #CR-165533, NASA Lewis Research Center, Cleveland, OH (1991).
14. Chan, K. S. & Lindholm, U. S., "Inelastic Deformation Under Nonisothermal Loading." ASME Journal of Engineering Materials and Technology, **112** (1990) 15-25.
15. Ramaswamy, V. G., Stouffer, D. C., & Laflen, J. H., "A Unified Constitutive Model for the Inelastic Uniaxial Response of Ren'e 80 at Temperatures Between 538°C and 982°C." ASME Journal of Engineering Materials and Technology, **112** (1990) 280-6.
16. Neu, R. W., "Nonisothermal Material Parameters for the Bodner-Partom Model." Paper presented at the Symposium on Parameter Estimation for Modern Constitutive Equations, ASME Winter Annual Meeting, New Orleans, LA, USA, 28 November - 3 December 1993.
17. Bodner, S. R., Partom, I., & Partom, Y., "Uniaxial Cyclic Loading of Elastic-Viscoplastic Materials." ASME Journal of Applied Mechanics, **46** (1979) 805-10.
18. Chan, K. S., Bodner, S. R., & Lindholm, U. S., "Phenomenological Modeling of Hardening and Thermal Recovery in Metals." ASME Journal of Engineering Materials and Technology, **110** (1988) 1-8.
19. Santhosh, U., Ahmad, J., & Nagar, A., "Nonlinear Micromechanics Analysis Prediction of the Behavior of Titanium-Alloy Matrix Composites." ASME Fracture and Damage, AD-Vol. **27** (1992) 65-76.
20. Mital, S. K. & Chamis, C. C., "Microfracture in High Temperature Metal Matrix Crossply Laminates." Report for Space Act Agreement C99066G, NASA Lewis Research Center, Cleveland, OH.
21. Brust, F. W., Newaz, G. M., & Majumdar, B. S., "Damage Development in Metal Matrix Composites Including Plasticity and Creep Effects." Presented at the 8th International Conference on Fracture (ICF-8), Kiev, Ukraine, June 1993.
22. Lissenden, C. J., Herakovich, C. T., and Pindera, M., "Life Prediction Methodology for Titanium Matrix Composites." Paper presented at the Symposium on Life Prediction Methodology for Titanium Matrix Composites, sponsored by ASTM, Hilton Head, SC, USA, 22-24 March 1994.

23. Robertson, D. D. & Mall, S., "A Micromechanical Approach for Predicting Time-Dependent Nonlinear Material Behavior of a Metal Matrix Composite." Thermomechanical Behavior of Advanced Structural Materials, ASME, AD-Vol 34 /AMD-Vol 173 (1993) 85-111.
24. Aboudi, J., Mechanics of Composite Materials - A Unified Micromechanical Approach. New York: Elsevier Science Publishing Co., 1991.
25. Robertson, D. D. & Mall, S., "Analysis of the Thermomechanical Fatigue Response of Metal Matrix Composite Laminates With Interfacial Normal and Shear Failure." Thermomechanical Fatigue Behavior of Materials: 2nd Volume, ASTM STP 1263, M. J. Verrilli & M. G. Castelli, Eds., ASTM, Philadelphia, 1995.
26. Robertson, D. D. & Mall, S., "A Nonlinear Micromechanics Based Analysis of Metal Matrix Composite Laminates." Composite Science and Technology, 58 (1994).
27. Robertson, D. D. & Mall, S., "Micromechanical Analysis of Metal Matrix Composite Laminates with Fiber-Matrix Interfacial Damage." Composites Engineering, Accepted for publication (1994).
28. Talreja, R., "Statistical Considerations." Fatigue of Composite Materials, K. L. Reifsnider, ed., New York: Elsevier Science Publishing Co., 1990.
29. Sendekyj, G. P., "Fitting Models to Composite Materials Fatigue Data." Test Methods and Design Allowables for Fibrous Composites, ASTM STP 734, C. C. Chamis, ed., ASTM (1981) 245-60.
30. Ramakrishnan, V. & Jayaraman, N., "Mechanistically Based Fatigue-Damage Evolution Model for Brittle Matrix Fibre-Reinforced Composites." Journal of Materials Science, 28 (1993) 5592-602.
31. Smith, K. N., Watson, P., & Topper, T. H., "A Stress-Strain Function for the Fatigue of Metals." Journal of Materials, JMLSA, 5 (1970) 767-78.
32. Gao, Z. & Zhao, H., "Life Predictions of Metal Matrix Composite Laminates Under Isothermal and Nonisothermal Fatigue." Journal of Composite Materials, Submitted for publication, 1994.
33. Nicholas, T. & Updegraff, J. J., "Modeling Thermal Fatigue Damage in Metal Matrix Composites."
34. Mirdamadi, M., Johnson, W. S., Bahei-El-Din, Y. A., & Castelli, M. G., "Analysis of Thermomechanical Fatigue of Unidirectional Titanium Metal Matrix Composites." NASA TM 104105, Presented at the ASTM Symposium of Composites Materials: Fatigue and Fracture IV, Indianapolis, IN, 6-9 May 1991.

35. Neu, R. W., "Characterization of Ti- β 21s with the Bodner-Partom (Directional Hardening Form) Constitutive Model." Presented to the NIC Steering Committee Meeting, Naval Research Laboratory, Washington, DC, 29-30 September 1992.
36. Neu, R. W. & Nicholas, T., "Effect of Laminate Orientation on the Thermomechanical Fatigue Behavior of a Titanium Matrix Composite." Journal of Composites Technology & Research, JCTRER, **16** (1994) 214-24.
37. Johnson, W. S., Lubowinski, S. J., & Highsmith, A. L., "Mechanical Characterization of Unnotched SCS-6/Ti-15-3 Metal Matrix Composites at Room Temperature." Thermal and Mechanical Behavior of Ceramic and Metal Matrix Composites, ASTM STP 1080, Kennedy, Moeller, and Johnson, Eds., 1990.
38. Wilt, T. E. & Arnold, S. M., "A Computationally-Coupled Deformation and Damage Finite Element Methodology." NASA Conference Publication 19117, Proceedings of the 6th Annual HITEMP, sponsored by NASA Lewis Research Center, Cleveland, OH, 25-27 October 1993.
39. Majumdar, B. S. & Newaz, G. M., "Fatigue of a SCS-6/Ti-15-3 Metal Matrix Composite." Paper presented at the American Society for Composites 8th Technical Conference, Cleveland, OH, 19-21 October 1993.
40. Castelli, M. G. & Gayda, J., "An Overview of Elevated Temperature Damage Mechanisms and Fatigue Behavior of a Unidirectional SCS-6/Ti-15-3 Composite." Paper presented at the 10th Biennial Conference on Reliability, Stress Analysis, and Failure Prevention, sponsored by ASME, Albuquerque, NM, 19-22 September 1993.
41. Pollock, W. D. & Johnson, W. S., "Characterization of Unnotched SCS-6/Ti-15-3 Metal Matrix Composites at 650°C." Composite Materials Testing and Design (10th Volume), ASTM STP 1120, G. C. Grimes, Ed., ASTM, Philadelphia (1992), 175-91.
42. Mall, S. & Schubbe, J. J., "Thermomechanical Fatigue Behavior of a Cross-Ply SCS-6/Ti-15-3 Metal Matrix Composite." Composites Science and Technology, **50** (1994) 49-57.
43. Hart, K. A. & Mall, S., "Thermomechanical Fatigue Behavior of a Quasi-Isotropic SCS-6/Ti-15-3 Metal Matrix Composite." Accepted for publication in ASME Journal of Engineering Materials and Technology (1994).
44. Roush, J. T., Mall, S., & Vaught, W. H., "Thermomechanical Fatigue Behavior of an Angle-Ply SCS-6/Ti-15-3 Metal Matrix Composite." Accepted for publication in Composites Science and Technology (1994).

Appendix A

Bodner-Partom Theory Computer Code

The following is the computer code that was used to produce the stress-strain curves in Section 4.1. The code is written in the language, C, and was compiled using Borland C/C++ version 4.0. The necessary code to run this algorithm as the function, *bodpart*, in MathCad is also included.

```
#include "mcadincl.h"
#include "math.h"

#define INTERRUPTED 1
#define INSUFFICIENT_MEMORY 2
#define MUST_BE_REAL 3
#define NUMBER_OF_ERRORS 3

// table of error messages
// sets up error table
// to allow user to interrupt by hitting Escape
// and ensures real values are used
char * myErrorMessageTable[NUMBER_OF_ERRORS] =
{
    "interrupted",
    "insufficient memory",
    "must be real"
};

//

LRESULT PredictStressStrainCurve(COMPLEXARRAY * const Answer,
    const COMPLEXARRAY * const DataArray,
    const COMPLEXARRAY * const ConstArray )

{
    unsigned int count, count1, iter;
    double dt, ElastStressRate, EpsDe, Z, StressTry, EpsDP, par, Z0, ttot;
    double J2, RT, EpsPDIJ, WPD, Q, dZ, dum, Q2, ZD, EpsDCal,
    DEpsDP, R, SigD;
    double Sold[4], EpsDel[4], Snew[4], DBeta[4], U[4], Beta[4], Beta0[4];
```

```

// rename input variables so the program is easier to follow:

double E, nu, D0, M1, Z1, R1, A1, M2, Z2, R2, A2, Z3, N, k, Incr;
double EpsFinal, EpsDot;
int Length;
Incr = ConstArray->hReal[2][0];
E = ConstArray->hReal[0][0];
nu = ConstArray->hReal[1][0];
D0 = ConstArray->hReal[0][1];
M1 = ConstArray->hReal[1][1];
Z1 = ConstArray->hReal[2][1];
R1 = ConstArray->hReal[0][2];
A1 = ConstArray->hReal[1][2];
M2 = ConstArray->hReal[2][2];
Z2 = ConstArray->hReal[0][3];
R2 = ConstArray->hReal[1][3];
A2 = ConstArray->hReal[2][3];
Z3 = ConstArray->hReal[0][4];
N = ConstArray->hReal[1][4];
k = ConstArray->hReal[2][4];
EpsFinal = dataArray->hReal[0][0];
EpsDot = dataArray->hReal[0][1];
// now determine length of stress vector:
Length = Incr+1;

//Ensure that MathCad has sufficient memory:
if ( !MathcadArrayAllocate( Answer, Length, 3, TRUE, FALSE))
    return INSUFFICIENT_MEMORY;
// now initialize all the variables to be used in the program

Answer->hReal[1][0] = 0.0;
ttot = EpsFinal/EpsDot;
dt = ttot/Incr;
Answer->hReal[2][0] = dt;
// now determine strain values
for (count=0; count <= Length; count++)
    Answer->hReal[0][count] = count*dt*EpsDot;
ElastStressRate = E*EpsDot;
for (count=1; count <= 3; count++)
    Sold[count] = 0.0;

EpsDel[1] = EpsDot;
EpsDel[2] = -1.0*nu*EpsDot;

```

```

EpsDel[3] = -1.0*nu*EpsDot;
// calculated effective inelastic strain rate
dum = sqrt(2.0/3.0*(pow(EpsDel[1],2.0)+
    pow(EpsDel[2],2.0)+pow(EpsDel[3],2.0)));
if (dum>pow(10,-8))
    EpsDe = dum;
else
    EpsDe = pow(10,-8);
    Z = Z2;
    Z0 = Z2;

for (count=1; count <= 3; count++ )
    {Beta[count] = 0.0;
    Beta0[count] = 0.0;}

// And now for the algorithm itself

for (count=1; count <= Incr+1; count++ )
    {StressTry = Answer->hReal[1][count-
        1]+ElastStressRate*dt;
    EpsDP=0.0;
    iter=1;
    par=10.0; // ensures that first iteration doesn't meet
        tolerance
    while (par>.001 && iter<100)
        {// check to see if the user has interrupted
        if (isUserInterrupted())
            {MathcadArrayFree (Answer);
            return INTERRUPTED;
            };
        Snew[1]=2.0/3.0*StressTry;
        Snew[2]=-1.0/3.0*StressTry;
        Snew[3]=-1.0/3.0*StressTry;
        J2=.5*(pow(Snew[1],2.0)+pow(Snew[2],2.0)
            +pow(Snew[3],2.0));
        RT=sqrt(3.0*J2);
        U[1]=1.0;
        U[2]=0.0;
        U[3]=0.0;
        EpsPDIJ=1.5*EpsDP*Snew[1]/RT;
        WPD=StressTry*EpsPDIJ;
        Q=-1.0*M1*WPD-A1*pow(Z1,1.0-R1)
            *pow(Z-Z2,R1)/Z;
        dZ=(M1*Z1*WPD+Z0*Q)/(1.0/dt-Q);

```

```

dum=sqrt(pow(Beta[1],2.0)+pow(Beta[2],2.0)
        +pow(Beta[3],2.0));
Q2=-1.0*M2*WPD-A2*pow(dum/Z1,R2-1.0);

for ( count1=1; count1<=3; count1++ )
    {DBeta[count1]=(M2*Z3*WPD*U[count1]
        +Beta0[count1]*Q2)/(1.0/dt-Q2);
    Beta[count1]=Beta0[count1]+DBeta[count1];}
Z=Z0+dZ;

if (Z<Z2)
    Z=Z2;
else
    if (Z>Z1)
        Z=Z1;
    ZD=Beta[1]*U[1]+Beta[2]*U[2]+Beta[3]*U[3];
    EpsDCal=2.0/sqrt(3.0)*D0*
        exp(-.5*pow((Z+ZD)/RT,2.0*N));
    DEpsDP=EpsDCal-EpsDP;
    if (DEpsDP<0)
        R=-1.0*DEpsDP/(DEpsDP-k*EpsDe);
    else
        R=DEpsDP/(DEpsDP+k*EpsDe);
    EpsDP += EpsDe*R;
    EpsPDIJ=1.5*EpsDP*Snew[1]/RT;
    SigD=E*(EpsDot-EpsPDIJ);
    StressTry=Answer->hReal[1][count-1]+SigD*dt;
    par=abs(DEpsDP/EpsDe);
    iter += 1;
    }
for (count1=1; count1<3; count1++)
    {Sold[count1]=Snew[count1];
    Beta0[count1]=Beta[count1];
    }
Z0=Z;
Answer->hReal[1][count]=StressTry;
Answer->hReal[2][count]=iter;
}

return 0;
}

// The remainder of the file registers the function bodpart with MathCad
FUNCTIONINFO bodpart =
{

```

```

// Name by which mathcad will recognize the function
"bodpart",

// description of "bodpart" parameters to be used
// by the Insert Function dialog box
"Data, Constants",

// description of the function for the Insert Function dialog box
"returns a nx2 array consisting of axial stress and strain",

// pointer to the executable code
// i.e. code that should be executed
// when a user types in "bodpart(Data, Constants)="
(LPCFUNCTION)PredictStressStrainCurve,

// bodpart(args) returns a complex array
COMPLEX_ARRAY,

// bodpart takes on 2 arguments
2,

// the 2 arguments are complex arrays
{ COMPLEX_ARRAY, COMPLEX_ARRAY }
};

// DLL entry point code

BOOL WINAPI DllEntryPoint (HINSTANCE hDLL, DWORD dwReason,
                          LPVOID lpReserved)
{
    switch (dwReason)
    {
        case DLL_PROCESS_ATTACH:

            //
            // DLL is attaching to the address space of
            // the current process.

            // register the error message table
            if ( CreateUserErrorMessageTable(
                hDLL, NUMBER_OF_ERRORS, myErrorMessageTable ) )
            // and if the errors register OK
            // go ahead and register user function

```

```
CreateUserFunction( hDLL, &bodpart );  
    break;  
  
    case DLL_THREAD_ATTACH:  
    case DLL_THREAD_DETACH:  
    case DLL_PROCESS_DETACH:  
  
        break;  
  
    }  
  
    return TRUE;  
}
```

```
#undef INTERRUPTED  
#undef INSUFFICIENT_MEMORY  
#undef MUST_BE_REAL  
#undef NUMBER_OF_ERRORS
```

Vita

Capt Mark A. Foringer was born on 6 February 1965 at Scott Air Force Base, Illinois. He graduated from W. T. Woodson High School in 1983 and entered undergraduate studies at the Massachusetts Institute of Technology. He graduated with a Bachelor of Science degree in Materials Science and Engineering in June 1987. He was commissioned on 31 May 1987 upon completion of the Reserve Officer Training Course. His first assignment was at Cape Canaveral Air Force Station as a Launch Vehicle Facilities Engineer. While at Cape Canaveral AFS, he earned a Master of Business Administration degree from the Florida Institute of Technology. In May 1993, he entered the School of Engineering, Air Force Institute of Technology.

Permanent Address: 301 Lakeland Dr.
 Hampton, VA 23669

REPORT DOCUMENTATION PAGE

Form Approved
OMB No. 0704-0188

Public reporting burden for this collection of information is estimated to average 1 hour per response, including the time for reviewing instructions, searching existing data sources, gathering and maintaining the data needed, and completing and reviewing the collection of information. Send comments regarding this burden estimate or any other aspect of this collection of information, including suggestions for reducing this burden, to Washington Headquarters Services, Directorate for Information Operations and Reports, 1215 Jefferson Davis Highway, Suite 1204, Arlington, VA 22202-4302, and to the Office of Management and Budget, Paperwork Reduction Project (0704-0188), Washington, DC 20503.

1. AGENCY USE ONLY (Leave blank)		2. REPORT DATE December, 1994		3. REPORT TYPE AND DATES COVERED Master's Thesis	
4. TITLE AND SUBTITLE VISCOPLASTIC CHARACTERIZATION AND FATIGUE MODELING OF TITANIUM BASED METAL MATRIX COMPOSITES				5. FUNDING NUMBERS	
6. AUTHOR(S) Mark A. Foringer, Capt, USAF					
7. PERFORMING ORGANIZATION NAME(S) AND ADDRESS(ES) Air Force Institute of Technology 2750 P Street WPAFB, OH 45433-6583				8. PERFORMING ORGANIZATION REPORT NUMBER AFIT/GAE/ENY/94D-5	
9. SPONSORING/MONITORING AGENCY NAME(S) AND ADDRESS(ES) Dr. Walter Jones AFOSR/NA Bolling AFB, DC 20332-0001				10. SPONSORING/MONITORING AGENCY REPORT NUMBER	
11. SUPPLEMENTARY NOTES					
12a. DISTRIBUTION/AVAILABILITY STATEMENT Approved for public release; distribution unlimited				12b. DISTRIBUTION CODE	
13. ABSTRACT (Maximum 200 words) Viscoplastic characterization and fatigue modeling of titanium-based metal matrix composites was accomplished by combining a unified viscoplastic theory, a nonlinear micromechanics model, and a linear damage accumulation model. First, Ti-15-3 was characterized using the Bodner-Partom viscoplastic theory. A micromechanics model was then employed in a linear damage accumulation fatigue model to predict the fatigue behavior of titanium based composites. The viscoplastic behavior predictions of the micromechanics model were used to eliminate separately defined time dependent terms in the fatigue model. Also, a new linear damage accumulation model was developed from the fatigue behavior of the composite constituents. Finally, it was found that the microstresses in the 0 degree ply could be used to accurately predict the fatigue behavior of a laminate containing these plies.					
14. SUBJECT TERMS Titanium Alloy Fatigue Life Metal Matrix Composite				15. NUMBER OF PAGES 101	
				16. PRICE CODE	
17. SECURITY CLASSIFICATION OF REPORT Unclassified		18. SECURITY CLASSIFICATION OF THIS PAGE Unclassified		19. SECURITY CLASSIFICATION OF ABSTRACT Unclassified	
				20. LIMITATION OF ABSTRACT UL	